Available online at www.sciencedirect.com

ScienceDirect

Geochimica et Cosmochimica Acta 301 (2021) 230–258

Geochimica et Cosmochimica Acta

www.elsevier.com/locate/gca

# Highly volatile element (H, C, F, Cl, S) abundances and H isotopic compositions in chondrules from carbonaceous and ordinary chondrites

Kei Shimizu [a,*], Conel M.O'D. Alexander [a], Erik H. Hauri [a], Adam R. Sarafian [b], Larry R. Nittler [a], Jianhua Wang [a], Steven D. Jacobsen [c], Ruslan A. Mendybaev [d]

[a] *Earth and Planets Laboratory, Carnegie Institution for Science, Washington, DC 20015, United States*
[b] *Science and Technology Division, Corning Incorporated, Corning, NY 14831, United States*
[c] *Dept. of Earth and Planetary Sciences, Northwestern University, Evanston, IL 60208, United States*
[d] *Dept. of Geophysical Sciences, University of Chicago, Chicago, IL 60637, United States*

Received 16 November 2020; accepted in revised form 2 March 2021; Available online 10 March 2021

**Abstract**

The partial pressures and isotopic compositions of volatiles present during chondrule formation can be constrained by the highly volatile element or HVE (H, C, F, Cl, and S) abundances and isotopic compositions in chondrules. Here we present the results of high spatial resolution and low background secondary ion mass spectroscopy (SIMS) analyses of the HVE concentrations and H isotopic compositions in type I and II chondrules in primitive ordinary chondrites Semarkona (LL3.00) and Queen Alexandra Range (QUE) 97008 (L3.05), and the primitive carbonaceous chondrite Dominion Range (DOM) 08006 (CO3.00). The HVEs in the chondrules primarily reside in the mesostases, in which the HVE contents and H isotopic compositions vary significantly ($H_2O$: 8–10,200 ppm, $CO_2$: 2.4–1170 ppm, F: 0.3–30 ppm, Cl: 0.07–175 ppm, S: 0.38–4400 ppm, δD: 77–15,000‰). To dissolve such HVE contents in a silicate melt requires significantly higher total pressures (up to 1900 bars), and in some cases requires anomalous gas compositions (CO dominated), compared to those expected from canonical conditions of chondrule formation ($\sim 10^{-3}$ bars, $H_2 + H_2O$ dominated). Rather, the enrichments of $H_2O$, $CO_2$, Cl, and F in the mesostases at the edges of some chondrules suggest that there were secondary influxes of HVEs into the chondrule mesostases from the surrounding matrix during parent body processes. Consistent with this, melt inclusions sealed in olivine phenocrysts have significantly lower HVE contents than the mesostases in contact with the surrounding matrix material. Further, the calculated diffusion distances of $H_2O$ in silicate glasses under the relevant conditions are comparable to the radii of the chondrules. The high δD values in the mesostases could have been generated through isotopic Rayleigh fractionation as a result of the loss of very D-poor $H_2$ generated from Fe metal oxidation by $H_2O$ in the parent bodies. Based on these results, we hypothesize that the bulk of the HVEs in the chondrules are secondary in origin. However, a small portion of the HVEs in chondrules could be primary, as there are low but measurable amounts of HVEs in the melt inclusions that are sealed in phenocrysts. Further, measured S contents in some chondrule mesostases agree with those predicted in a sulfide saturated silicate melt based on an experimentally calibrated thermodynamic model. We constrain the upper limits of primary HVEs in the chondrules based on the lowest measured HVE contents to minimize the effects of the secondary influx of HVEs (type I $H_2O$: 7–11 ppm, $CO_2$: 0.3–0.6 ppm, F: 0.1–0.2 ppm, Cl: 0.01–0.03 ppm, S: 0.3–60 ppm, and type II $H_2O$: 50–85 ppm, $CO_2$: 0.4–3 ppm, F: 0.04–2 ppm, Cl: 0.04–2 ppm, S: 190–260 ppm).


* Corresponding author at: Dept. of Geoscience, University of Wisconsin-Madison, Madison, WI 53706, United States.
*E-mail address:* kshimizu4@wisc.edu (K. Shimizu).

https://doi.org/10.1016/j.gca.2021.03.005
0016-7037/

*Keywords:* Chondrule formation; Parent body processes; Volatile elements; Hydrogen; Carbon; Chlorine; Fluorine; Sulfur

## 1. INTRODUCTION

Chondrites are undifferentiated meteorites that are thought to be one of the key building blocks of the terrestrial planets and may have supplied most of their H, N, and C, that are essential for habitability and life (Robert, 2001; Alexander et al., 2012; Marty, 2012; Halliday, 2013; Piani et al., 2020). Therefore, it is important to understand the origin of the volatile elements in the chondrites themselves, which will also provide fundamental constraints for the still poorly understood origin of chondrites as well as the dynamical processes that occurred in the early solar nebula (Deloule and Robert, 1995; Alexander et al., 2012; Piani et al., 2018; Fujiya et al., 2019). All chondrites are variable mixtures of three basic components: chondrules, refractory inclusions and matrix. Refractory inclusions are high temperature solid condensates from the nebular gas that probably formed close to the young Sun, and some are the oldest dated Solar System objects (MacPherson, 2014). The fine–grained matrix in the most primitive chondrites is composed of amorphous silicates, anhydrous minerals (olivine, orthopyroxene, metal, sulfides), phyllosilicates and organic matter. Chondrules, which are the focus of this study, are small roughly spherical (0.1–1 mm diameter) objects with igneous textures that formed at peak temperatures of ~1700–2100 K (Hewins et al., 2005) and comprise between roughly 30 vol.% and 80 vol. % of chondrites, with the exception of CI chondrites. The majority of chondrules are primarily composed of olivine and/or low Ca pyroxene, glassy or crystalline mesostasis (interstitial material), Fe-Ni metal, and sulfides. They are, therefore, some of the oldest Solar System 'rocks' having formed ~1–4 millions years after the formation of CV calcium-aluminum-rich inclusions (CAIs) (Kita and Ushikubo, 2012; Schrader et al., 2017; Tenner et al., 2019), although some may have formed even earlier (Bollard et al., 2019). While they evidently formed as molten droplets from predominantly silicate precursor materials, their formation conditions and heating mechanism(s) are still poorly constrained and highly debated.

Moderately and highly volatile elements in chondrites show patterns of depletions that are mainly functions of their condensation temperatures (e.g., Wai and Wasson, 1977; Wasson and Kallemeyn, 1988; Palme et al., 2014; Braukmüller et al., 2018; Alexander, 2019a,b), some of which are similar to Earth's depletion pattern (Palme and O'Neill, 2014). The origin(s) of these depletion patterns remain enigmatic, although it has been attributed to different mechanisms, such as mixing of depleted chondrules and volatile-rich CI-like matrix (Anders, 1964; Zanda et al., 2018; Alexander, 2019a,b) and partial condensation from a cooling nebular gas along with continuous removal of the gas (Wasson and Chou, 1974; Cassen, 1996; Ciesla, 2008). Chondrules have been shown to be relatively volatile depleted (e.g., Grossman and Wasson, 1983; Kong and Palme, 1999; Alexander, 2005; Ebel et al., 2018), and that they play an important role in generating the bulk volatile depletions in chondrites (Alexander, 2019a,b). Extensive volatile loss from chondrule melt droplets would be expected from estimates of temperature and pressure conditions if chondrules formed in nebular shocks (Desch and Connolly, 2002), current sheets (Joung et al., 2004), and X-winds (Shu et al., 1996). However, chondrules lack the systematic isotopic mass fractionations typically associated with evaporation (Davis et al., 2005; Ebel et al., 2018). Observations also indicate that, at least in ordinary chondrite chondrules, the concentrations of the moderately volatile element Na were relatively high and changed relatively little from the beginning of crystallization (Alexander et al., 2008; Hewins et al., 2012), in contrast to predictions for moderately dust enriched systems (Ebel and Grossman 2000). In addition, the S isotopic compositions of sulfides and the S contents of chondrule mesostases record relatively high S partial pressures during chondrule formation (Tachibana and Huss, 2005; Marrocchi and Libourel, 2013; Piani et al., 2016). These observations suggest that chondrules formed under anomalously high dust/gas ratios that suppressed evaporation, and that the volatile element fractionations could have been largely inherited from the chondrule precursors. Hence, a fundamental conflict exists between observation and the theoretical models with the former apparently requiring significantly higher pressures and dust/gas ratios than assumed or predicted by the latter. A reconciliation of this conflict is paramount for our understanding of the volatile element depletion patterns observed in chondrites.

Further complicating the interpretation of the volatile inventories of chondrules, Robert et al. (1987) conducted stepped pyrolysis analyses of chondrules from Chainpur (LL3.4), and found a wide range of isotopic compositions in the H released at different temperatures ($\delta D = -440‰$ released at <350 °C to +4100‰ released at >400 °C). In another pyrolysis study, Sears et al. (1995) found even higher D-enrichments of up to +7200‰ in chondrules from Semarkona (LL3.0). A subsequent secondary ion mass spectrometry (SIMS) study by Deloule et al. (1998) found high concentrations of water in chondrule phenocrysts of olivine (500–2100 μg/g, hereafter ppm) and pyroxene (400–9800 ppm) from Bishunpur (L/LL3.1) and Semarkona that also exhibited a large range in D/H ratios (−500‰ to +2000‰). The high water contents in chondrule phenocrysts were interpreted to result from the presence of hydrous alteration phases. Reasoning that hydrothermal circulation in a parent body would generate homogeneous D/H ratios in alteration products, Deloule et al. (1998) concluded that the alteration phases must have formed during chondrule formation. They also argued that the large D enrichments require an interstellar component in the ices, while the low D/H values come from a water component that isotopically exchanged with protosolar $H_2$. The later SIMS studies of Grossman et al. (2000) and Grossman et al. (2002) also found a large range in D/H ratio

(50–2300‰) and water concentrations (140–9800 ppm) in Semarkona chondrule mesostases, but these were interpreted to result from exchange between the chondrule mesostases and the water-bearing matrix during aqueous processes in the parent body, as well as terrestrial contamination. In a study of the bulk D/H analyses of chondrites, Alexander et al. (2010) argued that the high D/H ratios in the ordinary chondrites are due to the oxidation of Fe by water and loss of isotopically light $H_2$ during parent body alteration rather than an interstellar source. The recent SIMS study of Stephant et al. (2017) found large ranges of $H_2O$ contents in chondrule olivines (76–1051 ppm), pyroxenes (266–1796 ppm), and mesostases (2284–87,466 ppm) in the meteorites Paris (CM2), Renazzo (CR2), and Bishunpur (LL3.15), while the measured D/H ratios were relatively close to the terrestrial values (−398‰ to +366‰) compared to previous studies. In addition, Piani et al. (2020) used SIMS to measure the water contents and D/H ratios in the glassy mesostases of SAH 97096 (EH3.1–3.4) chondrules and found $H_2O$ concentrations of 2700–12,300 ppm and δD value of $-147 \pm 16$‰. They also measured the glassy mesostases of Vigarano and Kaba (both CV3s) chondrules and found average $H_2O$ concentrations of 330 $\pm$ 140 ppm and 210 $\pm$ 120 ppm, respectively, and δD value of $-261 \pm 25$‰ and $17 \pm 95$‰, respectively.

In summary, previous studies of H in chondrules have shown wide ranges of water contents and D/H ratios that have been interpreted either as primary signatures established during chondrule formation or as secondary signatures produced by parent body alteration processes as well as terrestrial contamination. If correct, the former interpretation would have profound implications for the conditions of chondrule formation, given how volatile H is. Hydrogen would have been a major element in the nebula and should have been trapped in chondrule phases during formation, but at least under canonical nebular conditions, solubility experiments of $H_2$ and $H_2O$ in silicate melts (e.g., Dixon et al., 1995; Hirschmann et al., 2012; Newcombe et al., 2017) suggest that the H abundances in chondrule melts would have been much lower than previously reported in chondrule mesostases (140 ppm to 8.7 wt.% from studies of Deloule et al., 1998; Grossman et al., 2000, 2002; Stephant et al., 2017; Piani et al., 2020). For example, with a $10^3 \times$ CI dust enrichment relative to the solar composition, an oxygen fugacity ($f_{O2}$) that is buffered at 1.2 log units below Fe-FeO (IW−1.2), and a total pressure of $10^{-3}$ bars (Ebel and Grossman, 2000), the predicted $H_2O$ concentration in a silicate melt is ~10 ppm (refer to Section 5.2.3 for details of calculation). Chondrule olivines and low-Ca pyroxenes in equilibrium with such melt would have $H_2O$ concentration of ~0.015 ppm and ~0.19 ppm, respectively (using olivine/melt and low-Ca pyroxene/melt partition coefficients of 0.0015 and 0.019, respectively from Hauri et al., 2006). These are also significantly lower than the $H_2O$ concentrations in chondrule olivines (76–2120 ppm) and pyroxenes (266–9818 ppm) reported by previous studies (Deloule et al., 1998; Stephant et al., 2017). On the other hand, if the secondary interpretation for the H contents and isotopic compositions of chondrules is correct, it will provide insights into the processes involved in the aqueous alteration of the chondrites.

In order to better constrain the origin(s) of H in chondrules, we have used high precision, high spatial resolution, and low background NanoSIMS techniques, in conjunction with petrologic characterization, to measure the H, C, F, Cl, and S contents, as well as the H isotopic compositions, of chondrules in the primitive ordinary chondrites Semarkona (LL3.00) and Queen Alexandra Range (QUE) 97008 (L3.05), and the primitive carbonaceous chondrite Dominion Range (DOM) 08006 (CO3.00). We refer to H, C, F, Cl, and S, the elements of focus of our study, as highly volatile elements (HVEs). The ultimate aim of our study is to provide additional constraints on the chondrule formation environments using the HVE contents and H isotopic composition in chondrules. However, before we can infer anything about chondrule formation conditions, we must first understand and exclude the potential complications presented by parent body processes (both aqueous alteration and thermal metamorphism). The three very primitive chondrites were chosen for this study to try to minimize the potential effects of parent body processes. Nevertheless, despite their primitive natures, all three meteorites are lithified rocks that show clear evidence for having experienced both some aqueous alteration and modest heating (Hutchison et al., 1987; Alexander et al., 1989; Grossman and Brearley, 2005; Davidson et al., 2019).

## 2. SAMPLES

We analyzed thin sections of the Semarkona (LL3.00; section #01-5081, National Museum of Natural History, Smithsonian Institution), QUE 97008 (L3.05; section #22, NASA Johnson Space Center), and DOM 08006 (CO3.00; section #91, NASA Johnson Space Center) meteorites. In addition, small fragments of mesostasis and phenocrysts of ~100 μm diameter were picked from powdered samples of these meteorites and mounted in In (indium metal) and polished with water-based alumina slurries with grit sizes down to 0.3 μm.

The primitive natures of the meteorites in this study are shown by the high and homogeneous Cr contents in their chondrule olivines that indicate low degrees of thermal metamorphism (Grossman and Brearley, 2005; Davidson et al., 2019). However, all three meteorites exhibit some evidence for the effects of aqueous alteration. In Semarkona, the replacement of Fe-metal by magnetite and Fe-carbide (Hutchison et al., 1987; Krot et al., 1997), the presence of hydrous minerals, such as smectite, and phases like calcite, and maghemite (Scott et al., 1981; Hutchison et al., 1987; Alexander et al., 1989; Krot et al., 1997) all provide clear evidence for aqueous alteration. The alteration mostly affected the matrix, but did also affect chondrules as indicated by the presence of altered metal blebs, bleached chondrules (Grossman et al., 2000), and the local occurrence of smectite in chondrule mesostases (Hutchison et al., 1987; Grossman and Brearley, 2005). Several lines of evidence point to QUE 97008 having been more metamorphosed than Semarkona (Grossman and Brearley, 2005; Kimura et al., 2008; Bonal et al., 2016). Estimates of the peak tem-

peratures experienced by Semarkona are ≤220–320 °C (Alexander et al., 1989; Rubin et al., 1999; Busemann et al., 2007), while for QUE 97008 they range from ~220–250 °C (Busemann et al., 2007) to as high as ~470 °C (Kimura et al., 2008). DOM 08006 appears to have experienced similar peak metamorphic temperatures to Semarkona (Bonal et al., 2016; Alexander et al., 2018b). The presence in the matrix of DOM 08006 of sub-100-nm metal, sulfide, olivine, and pyroxene suggests that it experienced limited aqueous alteration (Davidson et al., 2019), which is supported by the high concentration of presolar silicate grains in DOM 08006 (Nittler et al., 2018). There is, however, a small amount of magnetite and fayalitic olivine present in the matrix that suggests that there were some amount of aqueous alteration (Davidson et al., 2019).

## 3. METHODS

### 3.1. Electron microprobe microanalyses

Electron microprobe microanalyses (EPMA) of chondrule mesostases, phenocrysts, and high-Ca pyroxene overgrowths on phenocryst were made with the JEOL 8530F electron microprobe at the Earth and Planets Laboratory (EPL) Carnegie Institution for Science, with a 5 μm diameter defocused beam, 15 keV acceleration voltage, and 10 nA beam current. Olivine (Mg, Si, Fe), anorthite (Ca, Al), albite (Na), orthoclase (K), fluorapatite (P), pyrite (S), sodalite (Cl), $TiO_2$ (Ti), $MgCr_2O_4$ (Cr), Ni olivine (Ni), and $MnO_2$ (Mn) were used as standards, and ZAF matrix corrections were applied. The average relative analytical uncertainties (2σ) based on repeated analyses of a secondary standard (mid-ocean ridge basalt glass ALV519-4-1) were <3% for $SiO_2$, $Al_2O_3$, MgO, FeO, and CaO, <5% for $TiO_2$, and $Na_2O$, and 32% for $K_2O$.

### 3.2. Secondary ion mass spectrometry

The concentrations of HVEs (H, C, F, Cl, and S) in the standards, blank (Suprasil glass (H, C, F, and S), synthetic forsterite (Cl), and chondrule phenocrysts (Cl)), chondrule mesostases and phenocrysts were measured with the Cameca NanoSIMS 50L ion microprobe at EPL. The vacuum in the sample chamber of the NanoSIMS was always between $\sim 5 \times 10^{-10}$ torr and $\sim 8 \times 10^{-10}$ torr during the analyses. The vacuum during the analyses of the standards and blanks, or samples and blanks were the same because the blank materials were always present in the same sample holder as the standards or samples. The ~3 nA $Cs^+$ primary beam was accelerated to 16 keV and focused to a spot size of ~3 μm. Prior to each analysis, the standard and sample surface was pre-sputtered by rastering the primary beam over a 30 × 30 μm area for 10 minutes to remove the Au coat and sputter away the surface contamination. For the analysis, the raster was reduced to 20 × 20 μm and the analysis conducted in imaging mode with 64 × 64 pixels/image. The counting time was set to 244 μs per pixel such that acquisition of a single frame took one second, and 50 frames were collected in each analysis. The secondary ions $^{12}C^-$, $^{16}OH^-$, $^{17}F^-$, $^{30}Si^-$, $^{32}S^-$, and $^{35}Cl^-$ were simultaneously collected with entrance slit 3 and aperture slit 3. The mass resolving power (MRP, Cameca definition) was ~7000, sufficient to separate $^{17}O$ from $^{16}O^1H$ (MRP required = 4713). Neither beam blanking nor electronic gating were used as the scanning ion images make it possible to avoid contamination signatures during post-processing. The electron gun was used to compensate for the charge generated on the sample surface due to the implantation of $Cs^+$ ions and extraction of negatively charged secondary ions and electrons.

We used the L'image software (Larry Nittler, Carnegie Institution) to analyze the scanning ion images, which were corrected for counting system deadtime and beam drift. Ratios of the ion images were made to obtain ratio images of $^{12}C^-/^{30}Si^-$, $^{16}OH^-/^{30}Si^-$, $^{17}F^-/^{30}Si^-$, $^{32}S^-/^{30}Si^-$, and $^{35}Cl^-/^{30}Si^-$. In each analysis of standards and samples, data were taken from specific regions of interest (ROIs). For standards, the ROIs were chosen to avoid the edges of the images in the same manner as beam blanking or electronic gating. For the samples, ROIs were chosen that were on areas of glassy mesostasis or phenocryst that were well away from cracks and the edges of the image to avoid contamination. In order to correct the data for background, the ROIs selected for the samples and standards were imported on to the blank ion image (Suprasil glass), and the counts of ions in the ROIs in the blank image were subtracted from the same ROIs in sample and standard ion images. The standards for the H (reported as $H_2O$) calibration curves for olivine, orthopyroxene, and glass were determined based on the analyses of standards that were described in Hauri et al. (2002), Koga et al. (2003), and Bell et al. (2004) (olivines: SynFo100, SynFo68, CM#58, ROM-177, ROM-250#13, orthopyroxene: KBH-1, ROM-273, glass: ALV519-4-1, WOK28-3, 1833-11, 1846-12, 1833-1) (Fig. S1). The C (reported as $CO_2$), F, Cl, S calibration curves were based on the analyses of glass standards described in Hauri et al. (2002) (ALV519-4-1, WOK28-3, 1833-11, 1846-12, 1833-1) (Fig. S1). The uncertainties in the analyses of the samples were determined by propagating the errors from the counting statistics of the samples and blank as well as the calibration based on the concurrent analysis of a standard (ALV519-4-1).

The HVE detection limits (as defined by Long and Winefordner, 1983) were determined using replicate analyses of Suprasil glass (H, C, F, and S), synthetic forsterite (Cl), and chondrule phenocrysts (Cl). The Suprasil glass was measured during both the standard and sample analyses to determine the H, C, F, and S backgrounds and detection limits. The standard and sample In mounts all had Surpasil glass mounted in them. For the analyses of the thin sections, Suprasil glass mounted in a 10 mm In mount that was always in the same holder as the thin section. However, we were not able to use the Suprasil glass to determine the Cl background and detection limit due to its high Cl content of 1000–3000 ppm that is inherent to the material. Hence, we used measurements of synthetic forsterite during standard analyses to determine our Cl background and detection limit. During the sample analyses sessions, synthetic forsterite was not available in the 10 mm In mount.

Instead, chondrule phenocrysts (olivines/orthopyroxenes) in the sample In mount and thin sections were analyzed multiple times, and the lowest Cl contents measured were used to determine the Cl background and detection limit. The HVE backgrounds and detection limits determined during the standard and sample analyses sessions are very similar to each other, consistent with the similar vacuum in the sample chamber during the standard analyses and the sample analyses ($\sim 5 \times 10^{-10}$ torr to $\sim 8 \times 10^{-10}$ torr). The average HVE detection limits determined for the analytical sessions are 6 ppm for $H_2O$, 2 ppm for $CO_2$, 0.2 ppm for F, 0.1 ppm for S, and 0.03 ppm for Cl. Although the In mount containing the Suprasil glass was in the same sample holder as the thin section, one could speculate that the H, C, F, and S backgrounds that are constrained using Suprasil could underestimate those in the epoxy-bearing thin sections. An alternative way to assess the backgrounds in the thin section analyses is to use the chondrule phenocrysts (olivine/orthopyroxene) by assuming that they are "dry" or HVE-free. As shown in Appendix A, however, the minimum C, F, and S concentrations measured in the chondrule phenocrysts agree well with those measured in the Suprasil glass (Figs. S2 and S3). It is further shown in Appendix A that, while H concentrations measured in the chondrule phenocrysts are consistently higher than those measured in the Suprasil glass (Fig. S2), this is the case even when they are both mounted in the same In mount (Fig. S3). Hence, the higher H concentrations measured in chondrule phenocrysts than in the Suprasil are unlikely to be due to higher H backgrounds in the thin sections, but instead are due to the higher inherent H concentrations in the chondrule phenocrysts relative to those of the Suprasil glass. In addition, no systematic differences were observed between the HVE concentrations measured in the chondrule mesostases and phenocrysts in the thin section vs. the In mount (Table S1), supporting their similar HVE background levels. Hence, we use the analyses of Suprasil glass mounted in an In mount (in the same sample holder as the thin sections) to constrain the H, C, F, and S backgrounds in this study (refer to Appendix A for a more detailed discussion). The average relative uncertainties ($2\sigma$) are 8% for $H_2O$, 7% for $CO_2$, 12% for F, 6% for S, and 15% for Cl for the analyses of the Semarkona section, they are 6% for $H_2O$, 9% for $CO_2$, 6% for F, 6% for S, and 10% for Cl for the analyses of the QUE 97008 section, and they are 10% for $H_2O$, 30% for $CO_2$, 7% for F, 7% for S, and 16% for Cl for the analyses of the DOM 08006 section.

The D/H ratios in the standards, blank (Suprasil glass), chondrule mesostases and phenocrysts were measured in a similar manner as the HVEs using the Cameca NanoSIMS 50L at EPL. The vacuum in the sample chamber of the NanoSIMS was always between $\sim 5 \times 10^{-10}$ torr and $\sim 8 \times 10^{-10}$ torr during the analyses. As with the HVE analyses, the vacuum during the D/H analyses of the standards and blanks, or samples and blanks were the same because the blank materials were always present in the same sample holder as the standards or samples. The primary beam current was $\sim$1 nA $Cs^+$, and $H^-$ and $D^-$ were simultaneously collected with entrance slit 1 and aperture slit 1. The mass resolving power (MRP) was $\sim$3000. We used the L'image software to analyze the scanning ion image in the same manner as the HVE measurements. The instrumental mass fractionation (IMF, $\alpha_{SIMS} = (D/H_{meas})/(D/H_{true})$) was determined from repeated analyses of multiple standard glasses with a range of compositions to obtain the IMF for a range of matrix compositions. The uncertainty in the analysis of a sample was determined by propagating the errors from the counting statistics of the sample and blank as well as the IMF based on the concurrent analysis of a standard (ALV519-4-1). The IMF factor $\alpha_{SIMS}$ was constant within 37‰ ($2\sigma$) ($\alpha_{SIMS} = 1.08 \pm 0.04$). The raw average D/H ratio measured for ALV519-4-1 was $1.559 \times 10^{-4}$ ($2\sigma = 37‰$).

## 4. RESULTS

### 4.1. Textures

A total of 28 chondrules were analyzed in this study, of which 6 are from Semarkona, 13 are from QUE 97008, and 9 are from DOM 08006. The criteria for choosing these chondrules were that (1) they had the least evidence of parent body alteration (e.g., oxidized metal, alteration veins of Fe-Mg silicate material, etc.), and (2) had relatively large areas of glassy mesostases with relatively low abundances of quench crystals. Classification of the chondrules based on Mg# (Type I > 0.9; Type II < 0.9), texture and mineralogy (porphyritic olivine (PO) or porphyritic olivine-pyroxene (POP), etc.), shape, diameters, and other information are summarized in Table 1. The BSE images of selected chondrules are shown in Fig. 1.

The type I chondrules are mostly composed of olivine/orthopyroxene phenocrysts, mesostases, and metal grains. The textures of the mesostases range from clear glass to showing fine-grained quench crystals, optically and in backscattered electron images. There is no clear evidence of devitrification of glass from both optical and backscattered electron inspection of the chondrules. The mesostases and olivines/orthopyroxenes of some type I chondrules are veined by Fe-Mg silicate material. While these veins are observed in some QUE 97008 and Semarkona type I chondrules, they are less prevalent compared to those in DOM 08006. There are also cracks that go through the mesostases and olivines/orthopyroxenes, although it is unclear whether they are original features or features that formed during thin section preparation. The low-Ca pyroxene grains are often overgrown by high-Ca pyroxene, which also occurs as isolated grains in the mesostases of some chondrules. Metal grains occur both within the mesostases as well as within the olivine grains ("dusty" olivines). The pristine metal grains are mostly kamacite with some taenite. Metal grains in some chondrules show textural and compositional evidence of alteration/oxidation, such as the presence of magnetite, especially those close to the edges of the chondrules as well as those in contact with the aforementioned veins that cut through the mesostases/phenocrysts. The prevalence of metal alteration can be ordered DOM 08006 > QUE 97008 > Semarkona (Table 1).

Table 1
List of chondrules analyzed in this study, and their type, texuture, and other characteristics.

| Meteorite | Chondrule[a] | Type | Texture[b] | Diameter long (μm)[c] | Diameter short (μm)[c] | Shape[c] | Major phases[d] | Glass texture | Alteration | Sulfide locations |
|---|---|---|---|---|---|---|---|---|---|---|
| QUE 97008 | Q1 | I | BO | 557 | 524 | Spherical | Gl, ol, metal | Glassy | Veined, metal oxidized | – |
| | Q2 | I | PP | 583 | 510 | Spherical | Gl, low Ca-px, high Ca-px, metal | Glassy | Metal slightly oxidized | – |
| | Q3 | I | PP | 875 | 825 | Spherical | Gl, low Ca-px, high Ca-px, metal | Glassy, subhedral high Ca-px grains | Metal slightly oxidized | – |
| | Q4 | I | PP | 563 | – | – | Gl, low Ca-px, high Ca-px, metal | Glassy, subhedral high Ca-px grains | Metal slightly oxidized | – |
| | Q5 | II | POP | 1030 | 629 | Pear | Gl, ol, low Ca-px, high Ca-px, sulfide | Glassy, subhedral high Ca-px grains | Minimal | Interior (235 μm in) - Rim |
| | Q7 | II | PP | 571 | 435 | Pear | Gl, low Ca-px, high Ca-px, sulfide | Glassy | Sulfide slightly altered | Interior (230 μm in) - Rim |
| | Q9 | I | PO | 693 | 512 | Pear | Gl, ol, metal | Glassy | Metal slightly oxidized | – |
| | Q10 | II | BOP | – | 986 | – | Gl, ol, low Ca-px, high Ca-px, sulfide | Glassy | Sulfide slightly altered | Interior (490 μm in) - Rim |
| | Q16 | II | PP | – | – | – | Gl, low Ca-px, high Ca-px, sulfide | Glassy, elongate high Ca-px grains | Sulfide slightly altered | Interior(190 μm in) - Rim |
| | Q19 | II | PP | – | – | – | Gl, low Ca-px, high Ca-px, sulfide | Glassy, elongate high Ca-px grains | Heavy cracking in mesostasis | Throughout the mesostasis |
| | Q20 | II | PO | – | – | – | Gl, ol, sulfide | Glassy | Minimal | Interior(180 μm in) - Rim |
| | Q9In | II | – | – | – | – | Gl, ol | Glassy | Minimal | – |
| | Q22In | II | – | – | – | – | Gl, ol | Glassy | Minimal | – |
| Semarkona | S1 | I | PO | 1500 | 960 | Elongated | Gl, ol, metal | Glassy, elongate high Ca-px grains | Veined, metal oxidized | – |
| | S2 | I | PO | 560 | 473 | Spherical | Gl, ol, metal | Glassy | Minimal | – |
| | S3 | II | PO | 1170 | 609 | Elongated | Gl, ol, sulfide | Glassy, subhedral high Ca-px grains | Minimal | Interior (270 μm in) - Rim |
| | S4 | I | PO | 579 | 629 | Spherical with protrusion | Gl, ol, metal, low Ca-px, and high Ca-px og | Glassy, elongate high Ca-px grains | Minimal | – |
| | S5 | II | PO | 4900 | – | – | Gl, ol, sulfide | Glassy, subhedral high Ca-px grains | Sulfide altered | Interior (1265 μm in) - Rim |
| | S13In | I | BO | – | – | – | Gl, ol | Glassy | Minimal | – |
| DOM 08006 | D1 | I | POP | – | 441 | Spherical | Gl, ol, low Ca-px, metal | Glassy | Veined, metal oxidized | – |
| | D2 | I | POP | 596 | 588 | Spherical | Gl, ol, low Ca-px, high Ca-px, metal | Glassy | Veined, metal oxidized | – |

Table 1
Continued.

| Meteorite | Chondrule[a] | Type | Texture[b] | Diameter long (μm)[c] | Diameter short (μm)[c] | Shape[c] | Major phases[d] | Glass texture | Alteration | Sulfide locations |
|---|---|---|---|---|---|---|---|---|---|---|
| | D3 | I | POP | 430 | 417 | Spherical | Gl, ol, low Ca-px, high Ca-px, metal | Glassy, elongate high Ca-px grains | Veined, metal oxidized | – |
| | D4 | I | PP | 311 | 259 | Spherical with protrusion | Gl, low Ca-px, high Ca-px, metal | Glassy, elongate high Ca-px grains | Metal slightly oxidized | – |
| | D5 | I | PO | 275 | 202 | Elongated | Gl, ol | Glassy | Minimal | – |
| | D6 | II | PO | 262 | 200 | Square | Gl, ol, sulfide | Glassy | Minimal | Interior (70 μm in) - Rim |
| | D7 | I | PP | 513 | 419 | Pear | Gl, low Ca-px, metal | Glassy, elongate high Ca-px grains | Veined, metal oxidized | – |
| | D8 | II | PO | 218 | 178 | Spherical | Gl, ol, sulfide | Glassy | Minimal | Interior (52 μm in) - Rim |
| | D9 | I | PP | 684 | 565 | Irreggular | Gl, low Ca-px, metal | Glassy, elongate high Ca-px grains | Heavily veined, metal oxidized | – |

[a] Chondrules labeled with In are fragment of chondrule that was mounted in indium.
[b] PO – porphyritic olivine, BO – barred olivine, PP – porphyritic pyroxene, POP – porphyritic olivine pyroxene.
[c] Diameter and shape could not be determined for chondrules that are anomalously large (S-5), partially destroyed (Q-10), unclearly defiend (e.g., Q-16), or are fragments (eg.., S-13In).
[d] Gl – glass, ol – olivine, low Ca-px – low-Ca pyroxene high Ca-px – high-Ca pyroxene, og – overgrowth.

The type II chondrules are mostly composed of olivine/orthopyroxene phenocrysts, mesostases, and sulfide grains. There is also no clear evidence of devitrification of glass from both optical and backscattered electron inspection of the chondrules. There is less evidence of veins of Fe-Mg silicate material in the mesostases and olivines/orthopyroxenes of the type II chondrules compared to type I chondrules. However, there are similar amounts of cracks that go through the mesostases and olivines/orthopyroxenes as in the type I chondrules. Sulfide grains occur both within the mesostases as well as within the phenocrysts. The pristine sulfide grains are troilite, and they are located in the interiors of the chondrules. Some sulfides, particularly those closer to or at the edge of the chondrule, show evidence of oxidation due to aqueous alteration such as their association with magnetite.

### 4.2. Major and minor elements

The major and minor element compositions of the chondrule mesostases, phenocrysts, and clinopyroxenes (overgrowths and phenocrysts in mesostases) in this study are shown in Table S1. Their compositions are fairly similar to those observed previously in Semarkona (Fig. S4) (Jones and Scott, 1989; Jones, 1990, 1994; Alexander et al., 2008) (glass $SiO_2 = 43–72$ wt.%, $TiO_2 = 0.01–2$ wt.%, $Al_2O_3 = 7–33$ wt.%, $Cr_2O_3 = 0.004–0.86$ wt.%, $FeO = 0.08–14$ wt.%, $MnO = 0.001–0.7$ wt.%, $MgO = 0.2–35$ wt.%, $CaO = 0.4–25$ wt.%, $Na_2O = 0.007–8.8$ wt.%, $K_2O = 0.002–1.2$ wt.%, $P_2O_5 = 0.002–2.96$ wt.%, phenocryst Mg# = 0.41–1.00). Consistent with previously established observations of chondrules, type I chondrule olivine/orthopyroxene phenocrysts in this study have low FeO contents (maximum Mg# of 0.05). The type I chondrule olivine/orthopyroxene phenocrysts also do not show significant zonation in Mg# based on the BSE images as well as transect analyses of several phenocrysts in Semarkona. Type II chondrule olivine/orthopyroxene phenocrysts in this study show concentric zoning with outward increases in FeO contents, and FeO contents ranging in Mg# of 0.41–0.86.

DOM 08006 has the highest concentration of type I chondrules of the meteorites in our study. Its chondrule mesostases are also on average the most depleted in alkalis (e.g., Na, K) and enriched in refractories (e.g., Al, Ca) in this study. The chondrule mesostases in QUE 97008, the most rich of our samples in type II chondrules, are on average the most enriched in alkalis and depleted in refractories. Type I chondrule mesostases in DOM 08006 and Semarkona are compositionally similar to each other on average, although the most alkali-depleted extremes are found in DOM 08006. Relative to those in DOM 08006 and Semarkona, type I chondrule mesostases in QUE 97008 tend to be more alkali enriched and refractory depleted. Type II chondrule mesostases in DOM 08006 tend to be more alkali depleted than those in QUE 97008 and Semarkona. While the average composition of type II chondrule mesostases in QUE 97008 and Semarkona are similar to each other, the most alkali-enriched examples are found in QUE 97008. In summary, the degrees of alkali enrichment and refractory element depletion for both type I and II chon-

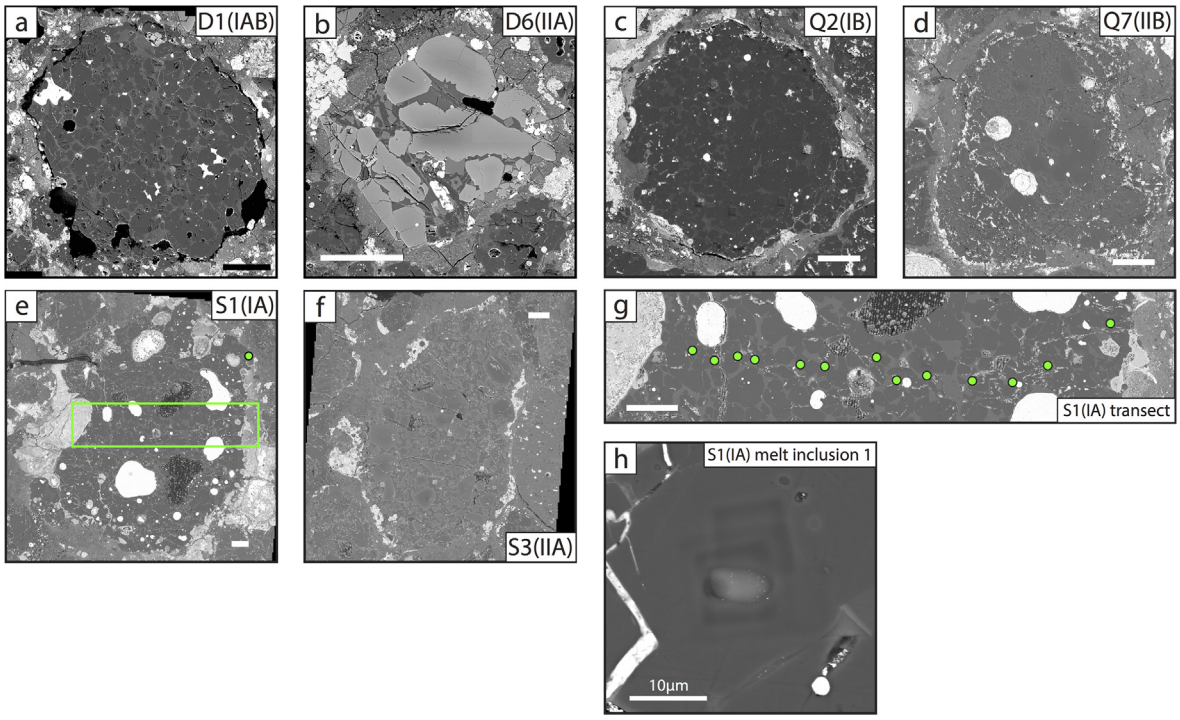


Fig. 1. BSE images of representative chondrules of (a, b) DOM 08006 (chondrules D1 and D6), (c, d) QUE 97008 (chondrules Q2 and Q7), and (e, f) Semarkona (chondrules S1 and S3). Also shown are (g) transect analyses spots (green dots) and (h) melt inclusion 1 in chondrule S1. Green box and dot in panel (e) indicates the location of panel (g) and (h), respectively. Scale bars are 100 μm, except for panel (h) in which it is 10 μm. (For interpretation of the references to colour in this figure legend, the reader is referred to the web version of this article.)

drules can be ordered QUE 97008 > Semarkona > DOM 08006.

Studies of Semarkona chondrules (Matsunami et al., 1993; Grossman et al., 2002; Alexander and Grossman, 2005; Nagahara et al., 2008) have shown that many type I chondrules have radially zoned mesostases, showing patterns such as increasing Na and decreasing Ca contents from the interior to surface. Of the three type I Semarkona chondrules in this study, two of them also show such zonation. Semarkona chondrule S2 in our study shows an increase in $Na_2O$ content from 0.5–2 wt.% in the interior to 4–6 wt.% at its surface (Fig. S5f), while its CaO content decreases from 12–13 wt.% to 10–8 wt.%. In addition to the outward zonation, there are "patchy" compositional heterogeneities in the chondrule mesostases, such as regions of high $Na_2O$ and $K_2O$. Similar to those in Semarkona, mesostases in type I chondrule of DOM 08006 show zonation patterns of increasing Na from the interior towards the surface, as well as "patchy" compositional heterogeneity. While the study of Grossman et al. (2002) observed little Na zonation in type II chondrules in Semarkona, we do observe zonation in Na contents in the type II chondrules in our study, although it is more complex as one chondrule shows Na increases towards the surface while another shows a decrease. In contrast, both the type I and II chondrule mesostases from QUE 97008 show less evidence of Na zonation, and they are more homogeneous in terms of the major and minor elements compared to those from Semarkona and DOM 08006.

### 4.3. Highly volatile elements or HVEs (H, C, F, Cl, S)

We report the H concentrations in the glassy mesostases (referred to as chondrule mesostases hereafter) and phenocrysts in the chondrules as $H_2O$ concentrations. The $H_2O$ concentrations in the chondrule mesostases measured in this study range from 8 ppm to 10,200 ppm (Fig. 2), and on average are lower than previous studies (62 ppm to 9 wt. %) (Deloule and Robert, 1995; Grossman et al., 2000, 2002; Stephant et al., 2017; Piani et al., 2020). Out of the three meteorites in this study, the chondrule mesostases with the highest average $H_2O$ concentrations are those in Semarkona, while the lowest are those in DOM 08006. The $H_2O$ concentrations in chondrule mesostases in QUE 97008 are more uniform within each chondrule compared to Semarkona and DOM 08006 chondrules. The range of $H_2O$ concentrations in the chondrule olivines and orthopyroxenes of 8–14 ppm in this study are also significantly lower than in previous studies (76–9818 ppm, Deloule et al., 1998; Stephant et al., 2017).

We report the C concentrations in the chondrule mesostases and phenocrysts as $CO_2$. The $CO_2$ concentrations in the chondrule mesostases measured in this study range from 2.4 ppm to 1170 ppm (Fig. 2), which is not significantly different from those observed in volcanic glasses found on Earth (e.g., Hauri et al., 2018). Similar to $H_2O$, the maximum average $CO_2$ concentration is observed in Semarkona chondrule mesostases, an intermediate concentration in QUE 97008 chondrules, and the lowest concentration in

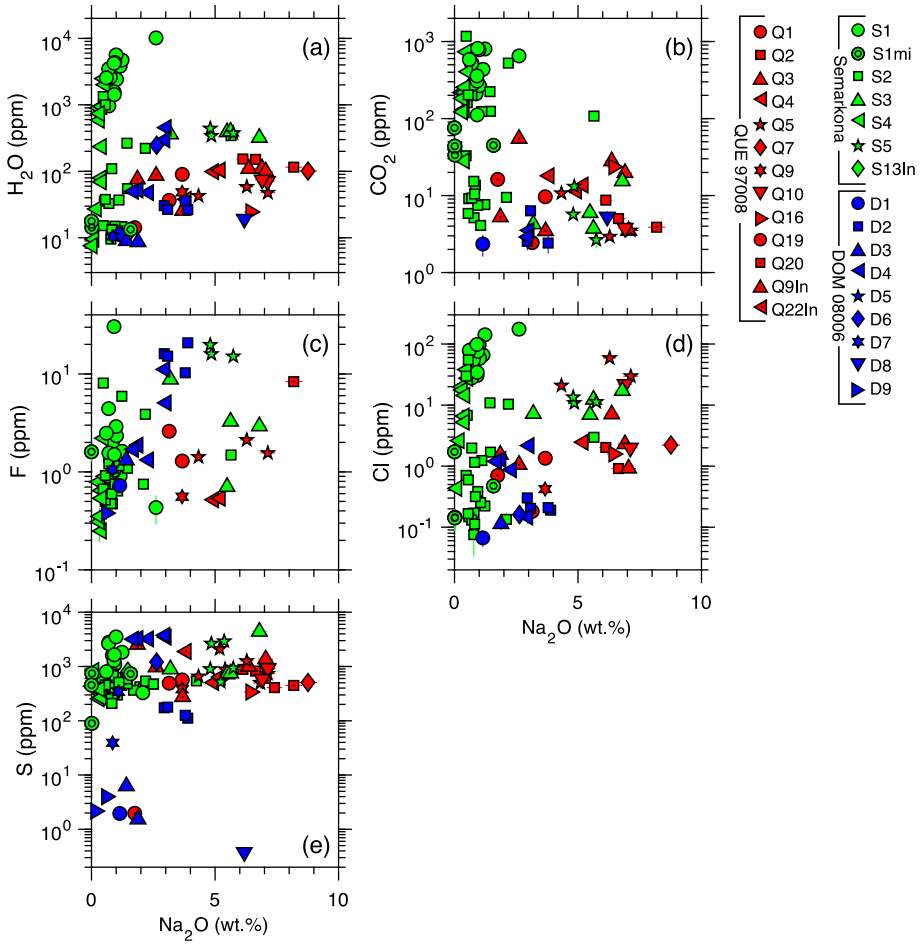


Fig. 2. (a) $H_2O$, (b) $CO_2$, (c) F, (d) Cl, and (e) S contents versus Na contents in the chondrule glassy mesostases of QUE 97008 (red), Semarkona (green), and DOM 08006 (blue). Symbols with the same shapes indicate that they are for the same chondrule. The green double circle symbols are melt inclusions in Semarkona chondrule S1. (For interpretation of the references to colour in this figure legend, the reader is referred to the web version of this article.)

DOM 08006 chondrules. The $CO_2$ concentrations in chondrule olivines/orthopyroxenes ranges from 2.8 ppm to 7 ppm. To our knowledge, this is the first determination of C concentrations in chondrule mesostases and phenocrysts.

The F and Cl concentrations in the chondrule mesostases fall in the ranges 0.3–30 ppm and 0.07–175 ppm, respectively (Fig. 2). These are, on average, lower than the previously reported F (2.9–807 ppm) and Cl (2.2–2690 ppm) concentrations in chondrule mesostases from Semarkona by Grossman et al. (2002). The chondrule olivines/orthopyroxenes have Cl concentrations in the range 0.04–0.07 ppm, while the F concentrations were below the detection limits (<0.2 ppm). Similar to $H_2O$ and $CO_2$, the average chondrule mesostases Cl concentrations are highest in Semarkona, intermediate in QUE 97008, and lowest in DOM 08006. In terms of F concentration in the mesostases, Semarkona and DOM 08006 overlap, while QUE 97008 is more depleted.

Sulfur concentrations in the chondrule mesostases fall in the range 0.38–4400 ppm (Fig. 2). The mid to upper portion of this range is comparable to those observed in previous studies (e.g., Marrocchi and Libourel, 2013; Piani et al., 2016). However, our results extend to significantly lower S concentrations due to the higher detection limits for S (e.g., 300 ppm, Piani et al., 2016) in previous EPMA studies compared to that in the SIMS measurements used here (0.1 ppm). We used the EPMA S data (detection limit = 200 ppm based on analyses of San Carlos olivine) for the chondrule mesostases for which we do not have SIMS S data. On average, the EMPA and SIMS S data on the chondrule mesostases agree to within 12% of each other. The S concentrations in the chondrule olivines/orthopyroxenes based on SIMS range from 0.14 ppm to 0.7 ppm. To our knowledge, this is the first determination of S concentrations in chondrule olivines/orthopyroxenes. The S contents in the chondrule mesostases are higher in the FeO-rich mesostases in the type II chondrules, compared to the FeO-poor mesostases in the type I chondrules. Hence, on average the S concentrations in the chondrule mesostases in DOM 08006 are low relative to those in QUE 97008 and Semarkona.

There are no clear correlations between HVE and $Na_2O$ concentrations in the chondrule mesostases (Fig. 2). How-

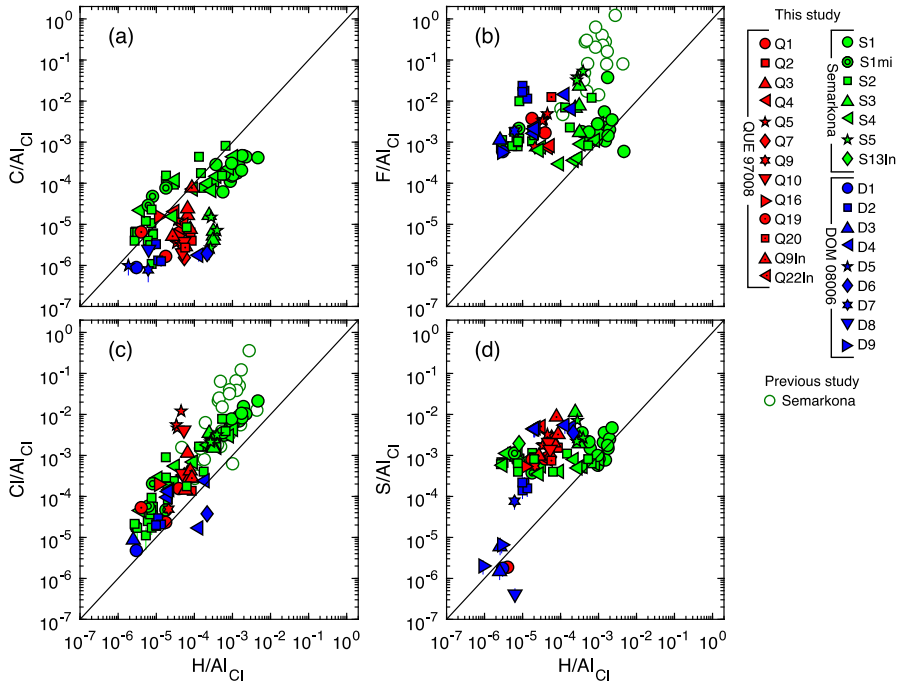


Fig. 3. The CI-normalized (a) C/Al, (b) F/Al, (c) Cl/Al, (d) S/Al versus H/Al ratios in the chondrule mesostases of QUE 97008 (red), Semarkona (green), and DOM 08006 (blue). The white circles with green borders are data from previous studies of Semarkona chondrule mesostases (Grossman et al., 2002). The CI composition is from Palme et al. (2014). The 1:1 solid line is plotted to guide the eye. (For interpretation of the references to colour in this figure legend, the reader is referred to the web version of this article.)

ever, when the type I Semarkona chondrules characterized by relatively low $Na_2O$ contents (<3 wt.%) are excluded, the chondrule mesostases with higher $Na_2O$ contents tend to have higher HVE contents, which is most clearly seen in $H_2O$ and Cl. The HVE contents in the type I Semarkona chondrules mesostases cover almost the entire range in the HVE contents that are observed in this study (Fig. 2). In terms of correlations amongst the HVEs, the strongest correlation is observed between $H_2O$ and Cl concentrations in the Semarkona chondrule mesostases (Fig. 3c).

Transect analyses of major and HVE abundances were conducted across the type I Semarkona chondrules (chondrules S1, S2, and S4). The transect analysis of chondrule S1 (Fig. 4 and Fig. 1g) shows that chondrule mesostases located closer to the edge of the chondrule have higher $H_2O$ and Cl contents, while the other HVEs do not seem to show such a trend. However, the transects of S2 and S4 shows that all HVEs in the chondrule mesostases tend to increase towards the edges of the chondrules (Fig. S5 and S6). The $H_2O$ and Cl contents in the chondrule mesostases of chondrules S1, S2, and S4 positively correlate with the FeO contents in the chondrule mesostases (Fig. 5a and b).

In the Semarkona chondrule S1, analyses were done on four glass inclusions that appear to have been enclosed within the phenocrysts prior to exposure at the surface of the thin section (Fig. 1h). Although it is uncertain whether or not the glass was completely enclosed within the phenocrysts due to the limited two-dimensional perspective, we tentatively refer to them as melt inclusions in this study. These melt inclusions are characterized by more than an order of magnitude lower $H_2O$ and Cl concentrations, relative to those of the chondrule S1 mesostases (Fig. 4). While the other HVE contents in these melt inclusions are less depleted, they tend to be close to or lower than the lowest HVE contents observed in the S1 chondrule mesostases (Fig. 4). The HVE contents in these melt inclusions are close to the lowest observed in all of the Semarkona chondrule mesostases, with the exception of $CO_2$ for which the mesostases in chondrules S2 and S4 show significantly lower $CO_2$ contents (Fig. 3a).

### 4.4. H isotopic compositions

The H isotopic compositions of the chondrule mesostases measured in this study range from $\delta D = 77‰$ to 15,000‰ (Fig. 6). The highest δD values are observed in the chondrule mesostases of QUE 97008, in which both type I and II chondrule mesostases show extremely high δD values of >10,000‰ (mean = 12,600 ± 2500‰, 2σ). All type IIs and some spots within the type I chondrule mesostases in Semarkona show similarly high δD values of >10,000‰, while the majority of type I chondrule mesostases have significantly lower δD values (<4000‰). In contrast, type II chondrule mesostases in DOM 08006 do not show as high δD values (maximum ~3000‰), although they are towards the higher end of the range observed in type I DOM 08006 chondrules mesostases (all DOM 08006 chondrule average = 1640 ± 2200‰, 2σ). The δD values observed in chondrule mesostases in this study significantly expand the range observed by previous studies

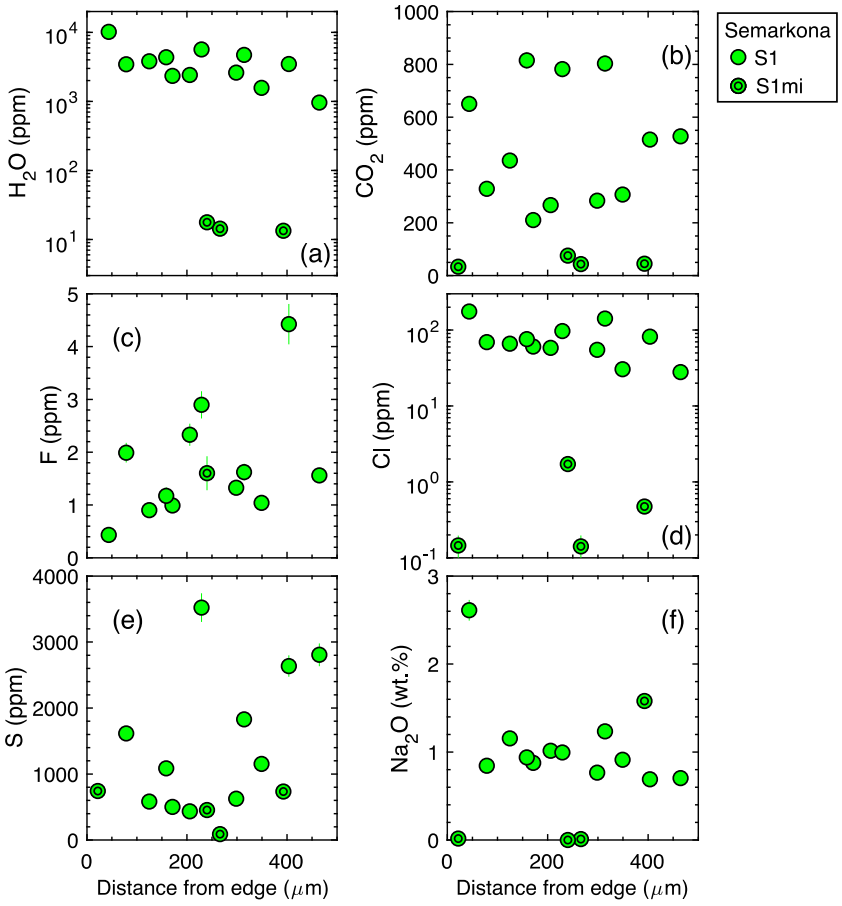


Fig. 4. Transect analysis of (a) $H_2O$, (b) $CO_2$, (c) F, (d) Cl, and (e) S concentrations in the mesostases (green circles) and melt inclusions (green double circles) in Semarkona chondrule S1. Certain HVE concentrations in some melt inclusions are not available due to being below our detection limits. (For interpretation of the references to colour in this figure legend, the reader is referred to the web version of this article.)

of −422‰ to 2340‰ (Deloule and Robert, 1995; Deloule et al., 1998; Grossman et al., 2000, 2002; Piani et al., 2020). In particular, our study is the first to observe extremely high δD values of >10,000‰ in chondrule mesostases. However, we did not observe the isotopically very light values reported in previous studies. When the δD values in the chondrule mesostases are plotted against their CaO contents, there is a stark difference observed in the δD values in QUE 97008 and Semarkona, where there is a sudden D-enrichment below a CaO content of ~12.5 wt.% (Fig. 7a). This corresponds to the CaO content below which chondrule mesostases are higher in $Na_2O$ (Fig. 7b), and the phenocrysts become more FeO enriched (i.e., more type II-like) (Fig. 7c).

## 5. DISCUSSIONS

The HVE concentrations and δD values measured in the chondrules in this study potentially reflect the pressures, dust/gas ratios and the isotopic composition of $H_2/H_2O$ in the chondrule formation regions. However, the effects of parent body processes on the HVE concentrations and D/H ratios in chondrules must be carefully evaluated. While the chondrules analyzed in this study are from primitive chondrites, previous studies have shown that parent body processes have affected the major and minor elements, as well as HVEs such as $H_2O$ and halogens, in chondrules (e.g., Grossman et al., 2002; Grossman and Brearley, 2005). Here we briefly summarize the disparate origins of moderate and HVEs in chondrules proposed in previous studies, then evaluate to what extent the HVEs measured in this study are secondary or primary in origin.

### 5.1. Secondary origin of moderate and HVEs in chondrules

#### *5.1.1. Previous evidences for the secondary alkalis, halogens, and water in chondrules*

The zonation of alkalis in the mesostases of type I chondrules in Semarkona has been interpreted to result from re-condensation of alkalis as chondrules cooled after formation (Matsunami et al., 1993; Nagahara et al., 2008) or from parent body aqueous alteration and metamorphism (Grossman et al., 2002; Alexander and Grossman, 2005; Grossman and Brearley, 2005). Matsunami et al. (1993) argued that aqueous alteration did not cause the Na zonation based on the apparent lack of alteration features in the chondrule glasses that they studied. In contrast, Grossman et al. (2002) argued against the re-condensation of alkalis

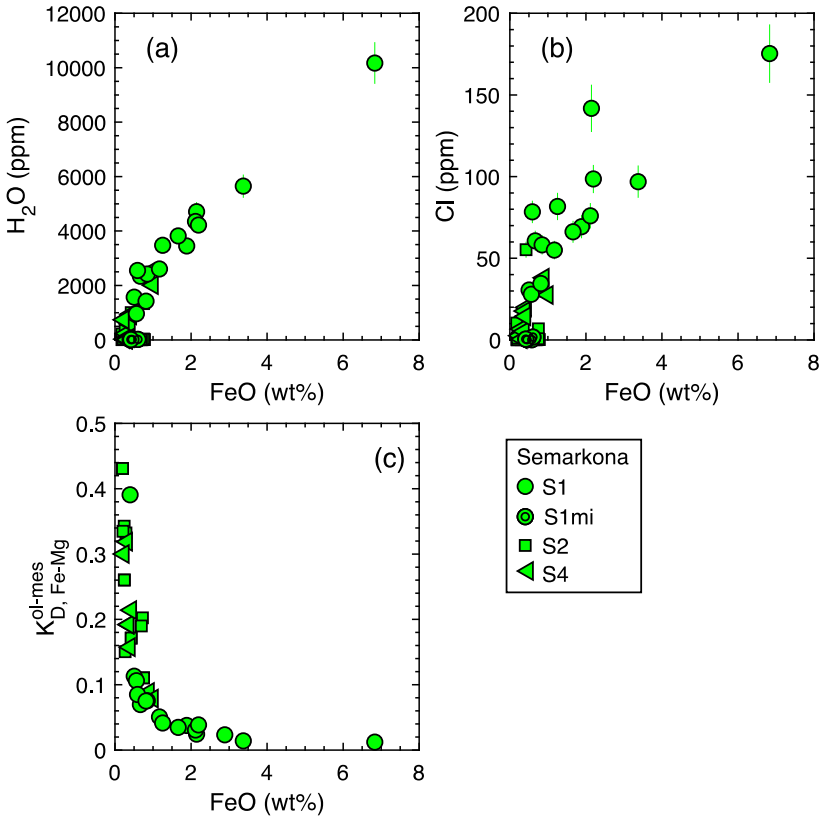


Fig. 5. (a) $H_2O$, (b) Cl contents in mesostases, and (c) Fe-Mg $K_d$ between mesostases and adjacent olivine phenocrysts versus FeO contents in the mesostases of type I Semarkona chondrules.

based on correlations between alkalis, halides and $H_2O$ concentrations, and the lack of Mg, Si, Cr, and Mn fractionation between the inner and outer zones of chondrules. Instead, they argued that the zonation of alkalis in the mesostases was due to exchange with fluids in the matrix that occurred in the LL parent body. Based on the evidence from terrestrial glasses (Mungall and Martin, 1994), they proposed that the chondrule glasses were altered through $Na^+$ and $H^+$ exchange and inward diffusion of molecular water without devitrification. Consistent with this scenario is the observation that in zoned type I chondrules in Semarkona, the high-Ca pyroxenes in or adjacent to mesostases have constant Na contents despite varying Na contents in the mesostases (Alexander and Grossman, 2005). High-Ca pyroxene-glass distribution coefficients of Na are consistent with experimentally determined igneous values only at the chondrule cores, and those closer to the rim are lower than igneous values. This suggests that Na in the zoned part of the mesostases surrounding the core was introduced after high-Ca pyroxene crystallization (Jones, 1994; Alexander and Grossman, 2005). Hence, while the alkalis in Semarkona chondrule mesostases at the chondrule cores may be primary in origin, those in zoned regions surrounding the chondrule core are likely secondary in origin.

In addition to Na, there is potential evidence of $H_2O$ diffusion into the chondrule mesostases based on the O isotopic disequilibrium between chondrule phenocrysts and mesostases. The study of Kita et al. (2010) found that the mesostases and phenocrysts from the same chondrules in Semarkona and two other primitive LL3s generally have distinct mass independently fractionated O isotopic compositions, with the mesostases compositions being more $^{16}O$-poor and trending towards that of matrix magnetite that is a product of aqueous alteration. They argued that low temperature O isotope exchange occurred in the LL parent body between chondrule glasses (but not phenocrysts) and higher $\Delta^{17}O$ aqueous fluids in the matrix. The experimental study of Behrens et al. (2007) supports this idea, as it showed that diffusion of $H_2O$ into a rhyolitic glass can alter its O isotopic composition without devitrifying the glass. Therefore, the O isotopic disequilibrium between chondrule phenocrysts and mesostases is secondary in origin, implying that the water that diffused in from the matrix overprinted whatever D/H ratios the chondrules may have had when they formed. Given that at least some of the $H_2O$ and alkalis in chondrule mesostases could be secondary in origin, we carefully evaluate the origins of the HVE concentrations and δD values measured in the chondrules in our study.

### *5.1.2. Anomalously high pressures of certain HVE species required during chondrule formation*

The $H_2O$, $CO_2$, F, Cl, and S contents in the chondrule mesostases in this study reach values of up to 10,200 ppm, 1170 ppm, 175 ppm, 30 ppm, and 4400 ppm,

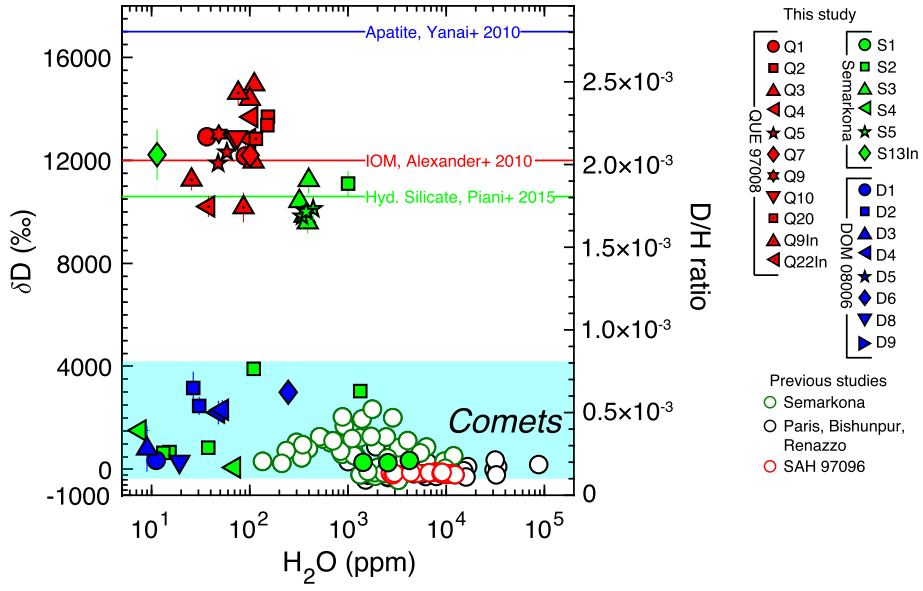


Fig. 6. The H isotopic compositions versus $H_2O$ contents in the chondrule mesostases of QUE 97008 (red), Semarkona (green), and DOM 08006 (blue). The white circles with green borders are data from previous studies of Semarkona chondrule mesostases (Deloule et al., 1998; Grossman et al., 2000, 2002), those with black borders are data from previous studies of Paris, Bishunpur, and Renazzo chondrule mesostases (Deloule et al., 1998; Stephant et al., 2017), and those with red borders are data from previous study of SAH 97096 chondrule mesostases (Piani et al., 2020). The H isotopic compositions of apatite from Ensisheim (LL6) (Yanai et al., 2012), IOM from WSG 95300 (H3.3) (Alexander et al., 2010), and hydrous silicates in the matrix of Semarkona (LL3.0) (Piani et al., 2015) are shown to illustrate the very high δD values found in other studies of ordinary chondrites. The range in H isotopic compositions of comets are from the compilation of Alexander et al. (2018a). (For interpretation of the references to colour in this figure legend, the reader is referred to the web version of this article.)

respectively, which are comparable to or even higher than those in some volcanic glasses and melt inclusions found on Earth (e.g., Hauri et al., 2018). This seems to be at odds with the high temperature and low pressure environment of nebular chondrule formation mechanisms such as shocks (Desch and Connolly, 2002), current sheets (Joung et al., 2004), and the X-wind (Shu et al., 1996). Even at the relatively high density ($10^3 \times$ CI dust enrichment, relative to the solar composition, $f_{O2}$ of IW−1.2) and pressure of $10^{-3}$ bars (Ebel and Grossman, 2000), the predicted $H_2O$ in the silicate melt is ~10 ppm (details of calculation discussed in Section 5.2.3). At the same pressure with a significantly higher dust enrichment of $10^5 \times$ CI ($f_{O2}$ of IW + 0.5), the predicted $H_2O$ in the silicate melt is only ~20 ppm. These are only consistent with the lowest $H_2O$ contents found in chondrule mesostases in this study. A more extreme condition (800 × CI and 1 bar) that has been invoked as a possible explanation for the high Na contents in chondrules at near liquidus temperatures may be able to dissolve ~100–1300 ppm $H_2O$ in the chondrule melt (Fedkin and Grossman, 2013), but this is still an order of magnitude lower than the highest values observed in our study.

We estimate the partial pressures of volatile species ($H_2$, $H_2O$, CO, and $CO_2$) in the gas phase that would be in equilibrium with the chondrule melt, to further emphasize that a primary interpretation of the higher $H_2O$ and $CO_2$ contents in the chondrule mesostases require anomalously high partial pressures in the chondrule forming regions. We use the experimentally determined relationships between the partial pressures of volatile species ($H_2$, $H_2O$, CO, and $CO_2$) in the gas phase and their concentrations in silicate melts ($CO_2$ (ppm) = 0.5 × $pCO_2$ (bar), Dixon et al., 1995; Eq. (6), Hirschmann et al., 2012; Eq. (10), Armstrong et al., 2015; Eq. (7), Newcombe et al., 2017). Further, we estimate the partial pressures in the gas phase using the reactions $H_2 + 0.5O_2 \Leftrightarrow H_2O$ and $CO + 0.5O_2 \Leftrightarrow CO_2$. Assuming a temperature of 1300 °C, we obtain the free energies of these reactions using the thermodynamic data from JANAF (Chase, 1998), and calculate the $f_{O2}$ using the empirical relationship between the $f_{O2}$ and chondrule Mg# from Tenner et al. (2015). The results suggest that gases in equilibrium with mesostasis melts would have total pressures of up to ~1900 bars, although most have total pressures of $10^{-2}$–$10^{1}$ bars (Fig. 8). The highest total pressures we predict are significantly higher than the pressures expected from nebular chondrule formation mechanisms (e.g., shocks, Desch and Connolly, 2002). Although it could be possible to reach such pressures, at least briefly, through planetesimal impact, the predicted compositions of the gases in equilibrium with the highest total pressure chondrule mesostases do not resemble those predicted for impact-generated atmospheres between chondritic planetesimals (Fig. S7) (Schaefer and Fegley, 2010).

While many of the chondrules with lower $H_2O$ and $CO_2$ contents have less anomalous predicted total pressures (<10 bars) (Fig. 8), they are still significantly higher than the canonical pressures of chondrule formation (~$10^{-3}$ bars). Nonetheless, these total pressures are comparable to the more extreme conditions that have been previously invoked to retain 50–90% of Na in the mesostases during chondrule formation (~0.08–25 bars, Fedkin and Grossman, 2013).

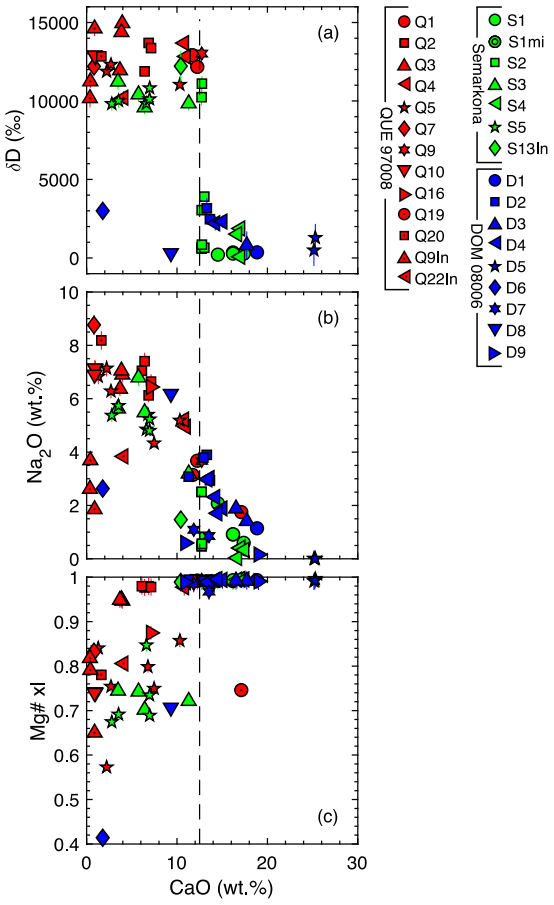


Fig. 7. (a) The H isotopic compositions, and (b) the $Na_2O$ contents in the chondrule mesostases, and (c) the Mg# in the chondrule phenocrysts versus the CaO contents in the chondrule mesostases of QUE 97008 (red), Semarkona (green), and DOM 08006 (blue). The vertical dashed line is drawn at a CaO content of 12.5 wt.%, below which there is a sudden D-enrichment. (For interpretation of the references to colour in this figure legend, the reader is referred to the web version of this article.)

For many of these chondrule mesostases with lower $H_2O$ and $CO_2$ contents, the predicted gas compositions are dominated by CO, while $CO_2$, $H_2$, and $H_2O$ are minor species (Fig. 8). This is in contrast to the $H_2$ and $H_2O$ dominated gas compositions predicted by Fedkin and Grossman (2013), and it is also unlike any impact-generated atmospheres from chondritic planetesimals (Schaefer and Fegley, 2010) (Fig. S7). Hence, the predicted gas compositions in equilibrium with the majority of the chondrules in this study are inconsistent with those in either nebular or planetesimal impact scenarios of chondrule formation. While some chondrule mesostases have $CO_2$ concentrations that are below our detection limit (2 ppm), it is unclear to what extent they are $CO_2$-free and therefore have $H_2$ and $H_2O$ dominated gas compositions predicted by chondrule formation models. Future studies of such chondrule mesostases with even lower detection limit $CO_2$ techniques are required to further evaluate this.

An alternative interpretation of the C contents in the chondrule mesostases is that it does not record the equilibrium solubility. Oxidation of reduced C from the chondrule precursors has been invoked for the generation of reduced type I chondrules, particularly those with dusty olivine grains containing metal inclusions (e.g., Connolly et al., 1994; Cohen and Hewins, 2004). In this process, $CO/CO_2$ will be generated and outgas from the chondrule, but this may be limited by how fast CO can diffuse through the chondrule melt. Hence, the C contents measured in the chondrule mesostases may record the disequilibrium process of incomplete CO loss (Hanon et al., 1998). However, at least in some chondrules, the C contents in the mesostases are enriched at the chondrule edge more than at the core (Figs. S5 and S6). This is contrary to the expectation from the incomplete CO loss scenario, in which the C in the mesostases would be enriched in the chondrule cores. While this does not completely rule out the incomplete diffusive CO loss scenario, it shows that other scenarios such as the secondary influx of C must also be investigated as a potential explanation of the C content in the chondrule mesostases.

### *5.1.3. Low temperature influxes of HVEs shown by transect and melt inclusion analyses of chondrules*

Transect and melt inclusion analyses of the HVEs in the type I chondrule mesostases in Semarkona suggests that there was a substantial secondary influx of HVEs into the chondrule mesostases. The concentrations of some HVEs tend to be higher in the chondrule mesostases closer to the edge of the chondrule (Fig. 4, Figs. S5 and S6), consistent with the observation of Grossman et al. (2002). In addition, the melt inclusions in chondrule S1 tend to have lower HVEs contents than the chondrule mesostases (Fig. 4). This is particularly the case for $H_2O$ and Cl that are more than an order of magnitude lower in the melt inclusions than in the chondrule mesostases. Given the high concentrations of volatile elements including H, halogens and alkalis in the matrix and chondrule rims (e.g., Grossman and Wasson, 1985; Alexander, 1995), our observations are most simply explained if most of the $H_2O$ and halogens were introduced into the chondrule mesostases during parent body alteration. Compared to the mesostases, the lower $H_2O$ contents in the melt inclusions suggest that they have been protected to a large extent by the surrounding olivine from the secondary influx of $H_2O$. This interpretation is supported by the aforementioned observation of mass independent O isotopic disequilibrium between the chondrule mesostases and phenocrysts that is likely due to low temperature O isotopic exchange between chondrule glasses (but not phenocrysts) and higher $\Delta^{17}O$ aqueous fluids in the matrix (Kita et al., 2010). Although, to our knowledge, chondrule melt inclusions have not been analyzed for their O isotopic compositions, our observations suggest that melt inclusions should show less or no O isotopic disequilibrium with the phenocrysts compared to the mesostases.

In addition to the O isotopic compositions, there is strong evidence that parent body processes have significantly altered the major element compositions of the

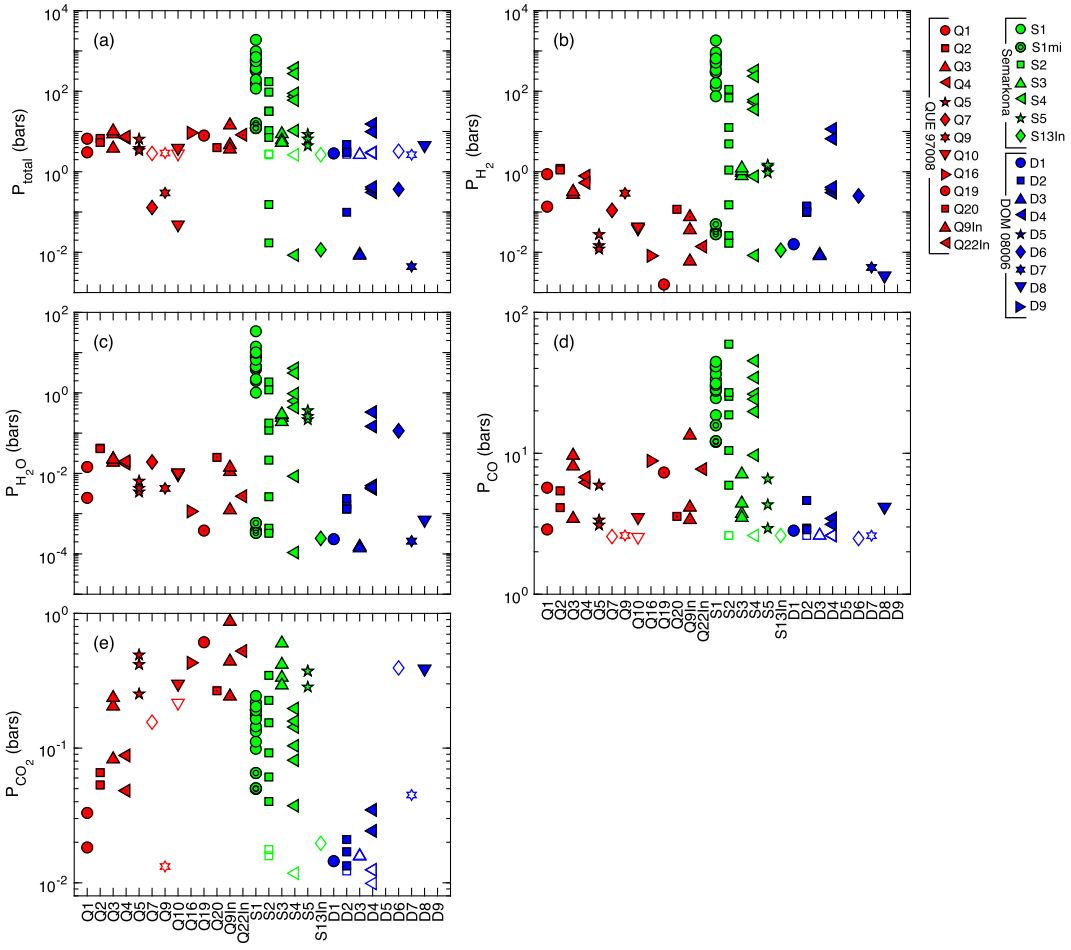


Fig. 8. The calculated (a) total pressure and partial pressures of (b) $H_2$, (c) $H_2O$, (d) CO, and (e) $CO_2$ in the vapors in equilibrium with the chondrule mesostases. The open symbols show the upper limits of the (a) $P_{total}$, (d) $P_{CO}$ and (e) $P_{CO2}$ of the chondrule mesostases with $CO_2$ concentrations that are below our detection limit of 2 ppm. Refer to Section 5.1.2 for details of the calculations.

chondrule mesostases in type I Semarkona chondrules. $H_2O$ and Cl concentrations in the mesostases positively correlate with the FeO contents in the mesostases in the Semarkona chondrules S1, S2, and S4 (Fig. 5a and b). Further, there is a negative correlation between the FeO contents in the mesostases and the Fe-Mg $K_d$ (defined as $(Fe/Mg)_{olivine}/(Fe/Mg)_{melt}$ where Fe and Mg are atomic concentrations) between the mesostases and the adjacent olivine phenocrysts (Fig. 5c). The observed range in Fe-Mg $K_d$ values is consistent with the previous observations that values $\ll 0.3$ are commonly observed in type I chondrules (e.g., Jones and Scott, 1989). This is in contrast to the equilibrium Fe-Mg $K_d$ between olivine and melt of 0.3 that has been experimentally shown to be valid for a range of melt temperatures and compositions (Roeder and Emslie, 1970). Rapid cooling experiments (Kennedy et al., 1993; Nettles et al., 2006) and oxidation experiments (Villeneuve et al., 2015) have been able to generate Fe-Mg $K_d$ values of 0.1–0.3. The Fe-Mg $K_d$ values in the low FeO Semarkona chondrule mesostases are mostly within 0.1–0.3 that is predicted from these experiments (Fig. 5c). In contrast, the Fe-Mg $K_d$ values in the high FeO mesostases are significantly lower than 0.1 and the range of 0.1–0.3 predicted from the rapid cooling/oxidation experiments. The positive correlations between the $H_2O$, Cl and FeO contents in the mesostases (Fig. 5a and b) suggest that the anomalously low Fe-Mg $K_d$ values ($\ll 0.1$) in the type I Semarkona chondrules are due to secondary influxes of FeO along with $H_2O$ and Cl into the mesostases. Although the details of the influx mechanism is out of the scope of this study, our observation are consistent with the hypothesis that diffusion of $H_2O$ and cation exchange between $Na^+$ and $H^+$ in chondrule glasses modified the glass structures and allowed other cations, including FeO, to diffuse into the glass from the matrix/fluid, similar to the processes observed in the alteration of terrestrial trachytic glass (Mungall and Martin, 1994).

The evidence for secondary influxes of FeO that is coupled with influx of $H_2O$ and Cl into the mesostases is less clear, however, in the type I chondrules of QUE 97008 and DOM 08006 and the type II chondrules (Fig. S8a and b). For example, while the mesostases of some type I chondrules in QUE 97008 have relatively high FeO (up to 2 wt.%), they have low and constant $H_2O$ (80–160 ppm) and Cl (1–5 ppm) contents unlike the high FeO mesostases in type I Semarkona chondrules (Fig. S8a and b). While this

may suggest minimal coupled secondary influx of FeO, $H_2O$, and Cl into the chondrule mesostases of QUE 97008 and DOM 08006, this does not rule out the secondary origin of their $H_2O$ and Cl. The stronger evidence of secondary influxes of $H_2O$ and Cl in Semarkona suggest the greater degree of aqueous alteration it experienced than QUE 97008 and DOM 08006.

#### *5.1.4. Diffusion distance of H in glass supports the secondary origin of $H_2O$*

It is clear from the transect and melt inclusion analyses of HVEs combined with the O isotopic phenocryst-mesostasis disequilibrium (Kita et al., 2010) that there was an influx of HVEs into chondrule mesostases after formation of chondrules. The plausibility of this having occurred in their parent bodies would be enhanced if it can be shown that the diffusivity of $H_2O$ in glass is rapid enough at relatively low temperatures to explain the concentration profiles observed in the chondrules. We have extrapolated the $H_2O$ diffusivities in silicate melts of different compositions from Zhang and Ni (2010) to estimate the diffusivity of $H_2O$ in glasses of these compositions. We use this approach since the constraints on diffusivity of $H_2O$ in glasses of relevant composition are relatively sparse, although there are studies on $H_2O$ diffusion in rhyolitic (e.g., Zhang and Behrens, 2000) and commercial glasses (Doremus, 1994). The study of Hudak and Bindeman (2020), however, suggests that the diffusivity of $H_2O$ in rhyolitic glass at relatively low temperatures can be up to 5.5 times greater than extrapolated from high temperature experiments in melt and glass (Zhang and Behrens, 2000). Hence, the diffusivity of $H_2O$ in glasses of different compositions estimated in this study through extrapolation from $H_2O$ diffusivities in silicate melts may be minimum estimates. We used a temperature of 300 °C to calculate the $H_2O$ diffusivities (Fig. S9a and b), which is consistent with the upper limits for the peak temperatures experienced by Semarkona and DOM 08006, but may be too low for QUE 97008 (Alexander et al., 1989; Rubin et al., 1999; Busemann et al., 2007). The duration of alteration/metamorphism experienced by type 3.0–3.1 chondrites is poorly constrained. Assuming a nominal 1 Myr timescale, the estimated diffusivities indicate that diffusion distances would have been significantly greater than (e.g., rhyolite) or comparable to (e.g., andesite) the chondrule diameters in our samples (Fig. 9), lending plausibility to the $H_2O$ in the chondrule mesostases being secondary in origin. The calculated $H_2O$ diffusivities show that $Na_2O$- and $SiO_2$-rich rhyolitic glasses should have higher diffusivities than andesitic and basaltic glasses (Fig. S9a and b). In fact, the $H_2O$ and $Na_2O$ contents in the relatively low $H_2O$ chondrules ($H_2O < 160$ ppm) in QUE 97008 and DOM 08006 appear to positively correlate with each other (Fig. S9c). This would be consistent with the faster diffusivity of $H_2O$ in $Na_2O$-rich glass (Fig. S9b), or alternatively, glasses with higher $Na_2O$ contents may have a greater capacity for $H_2O$ that is perhaps related to the cation exchange between $Na^+$ and $H^+$ in glass (Mungall and Martin, 1994). In addition, the O isotopic differences between the glasses and phenocrysts in Semarkona chondrules (Kita et al. (2010) are

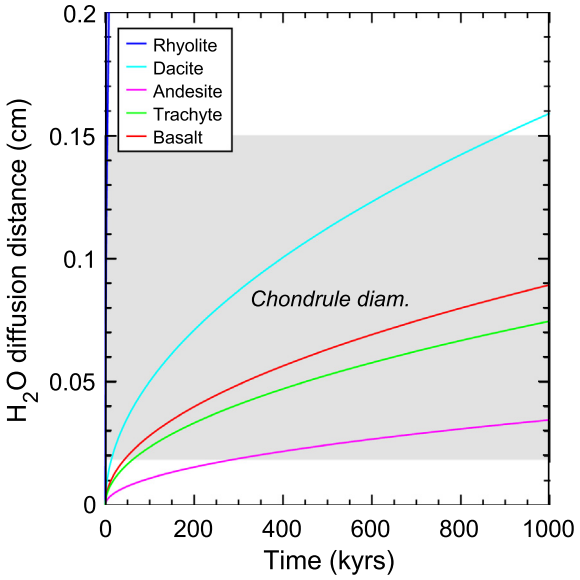


Fig. 9. The $H_2O$ diffusion distances in glasses of different compositions calculated using the diffusion coefficients of Zhang and Ni (2010), assuming a temperature of 300 °C and an alteration/metamorphic timescale of up to 1 Myr.

significantly larger for type II than type I chondrules, implying that type II chondrule mesostases were able to exchange O isotopes to a greater extent (Fig. S10). This is consistent with our hypothesis that the higher $Na_2O$ and $SiO_2$ glasses in type II chondrules should have a higher $H_2O$ diffusivity compared to the glasses of type I chondrules. The $Na_2O$ content of the glass, however, is not the sole control on the degree of secondary $H_2O$ enrichment since some low $Na_2O$ chondrule mesostases are highly enriched in $H_2O$ (Fig. 2a). The positive correlations between $H_2O$, Cl and FeO contents in low Na type I Semarkona chondrules (Fig. 5) suggests that multiple factors must have played roles in determining the secondary $H_2O$ contents of chondrule mesostases.

#### *5.1.5. Extremely high δD values (>10,000‰) in chondrule mesostases are difficult to explain as primary δD signature*

The δD values in the chondrule mesostases also point to the secondary origin of H in chondrule mesostases. The high δD values of chondrule mesostases in QUE 97008 ($12600 \pm 2500$‰ ($2\sigma$)) as well as the type II chondrule mesostases of Semarkona ($10{,}400 \pm 770$‰ ($2\sigma$)) are difficult to reconcile with a primary origin for the H (Fig. 6). Similarly high δD values have been observed in organic material (Alexander et al., 2010), matrix phyllosilicates in Semarkona (Piani et al., 2015), and phosphates (Yanai et al., 2012) in ordinary chondrites (Fig. 6). However, our study is the first to measure high δD values of greater than 10,000‰ in chondrule mesostases as the highest δD values from previous studies are $2075 \pm 50$‰ (Deloule et al., 1998) and $2340 \pm 300$‰ (Grossman et al., 2002). Grossman et al. (2002) interpreted the δD value to originate from the secondary influx of H from the D-rich matrix into the mesostases. On the other hand, Deloule et al. (1998) proposed

that what now appear to be their moderately high δD values in chondrule mesostases were inherited from chondrule precursors that contained some amount of D-rich molecular cloud ices. Irrespective of the difficulties of retaining any $H_2O$ from the precursors during chondrule formation (Sections 5.1.2 and 5.2.3), to explain the δD values >10,000‰ that we observe requires that the water in the precursors were dominated by molecular cloud ices. This may not be impossible, but it seems unlikely. The ordinary chondrite formation regions are thought to have been in the warmer inner Solar System, and those of the carbonaceous chondrites in the cooler outer Solar System (e.g., Warren, 2011; Budde et al., 2016; Kruijer et al., 2017). Isotopic re-equilibration of $H_2O$ is predicted to have been more extensive in the inner Solar System (e.g., Horner et al., 2007; Yang et al., 2013). Yet, the δD values in DOM 08006 do not come close to 10,000‰. Furthermore, the initial bulk δD of the water in Semarkona was at most 799–1210‰, and likely even lower (−527‰ to 154‰) considering the effect of Fe metal oxidation and loss of D-poor $H_2$ gas (Alexander et al., 2010; Sutton et al., 2017). Therefore, the water in the ordinary chondrite formation region would have had to drastically change from extremely D-rich during chondrule formation to relatively D-poor at the time of accretion of the LL chondrite parent body. The δD values in the type I chondrules in Semarkona (77–3900‰) and those in DOM 08006 (300–3200‰) are significantly lower, although some are still quite D-rich. This range in δD values is similar to those observed in comets. However, this is likely a coincidence as the bulk δD value of water accreted by Semarkona's parent body was probably significantly lighter (−527‰ to 154‰, Sutton et al., 2017), and that accreted by the parent body of DOM 08006 probably also light (<−64‰ to −57‰, Alexander et al., 2018b). This again, would require that the water in the chondrule formation regions were significantly more D-rich than the water that accreted onto the parent bodies. Hence, while it may not be impossible, it is difficult to argue that the H and D/H ratios in the chondrule mesostases are primary (i.e., predate accretion).

We consider a secondary origin scenario for the elevated δD values in the chondrule mesostases more likely. If the water in the matrix diffused into the chondrule mesostases, as discussed above, their δD values are the signatures of the water that was present in the parent bodies when the mesostases effectively closed to diffusive exchange with the matrix. The wide range of compositions and often larger D enrichments in the water could originate from ice grains with heterogeneous isotopic compositions that accreted onto the parent bodies (Deloule et al., 1998; Piani et al., 2015), but this would require that ordinary chondrites accreted more molecular cloud ice than carbonaceous chondrites like the COs (Alexander et al., 2012).

The D-enrichments in the water instead may be the products of isotopic exchange between $H_2O$ and D-rich organics, and isotopic Rayleigh fractionation as a result of the loss of very D-poor $H_2$ generated by Fe metal oxidation by $H_2O$ ($3Fe + 4H_2O \Leftrightarrow Fe_3O_4 + 4H_2$) (Alexander et al., 2010; Bonal et al., 2013; Sutton et al., 2017). After about 96% loss of H, the residual $H_2O$ can reach a δD value of 12,000‰, assuming an initial δD value of 0% and a temperature of 0 °C (~99% loss if 100 °C is assumed). This amount of H loss is large, and greater than the 73–83% H loss estimated for Semarkona based on its bulk Fe oxidation state (Sutton et al., 2017). The 73–83% H loss is, however, a bulk or average loss for the meteorite and locally fractional losses could have been significantly higher, particularly if water was continuously being sequestered into secondary minerals that did not continue to exchange with the remaining fluid. The D-rich water generated through the isotopic Rayleigh fractionation process then diffused into the chondrule mesostases (Sections 5.1.3 and 5.1.4). Some oxidation of Fe (as metal, FeS and, perhaps, FeO) could even have occurred in the mesostasis itself.

As discussed earlier, the high δD values are found in chondrule mesostases with relatively high $Na_2O$ contents (Fig. 7) in which $H_2O$ can diffuse faster (Fig. S9b), which is consistent with them closing later after more extensive $H_2O$ loss had occurred. Semarkona chondrule mesostases, however, display a considerable range in δD values. If the δD values are secondary features, then the range in H isotopic compositions requires that chondrules record different stages of H loss or mixing between fractionated and unfractionated reservoirs of H. The fact that type I chondrule mesostases typically have lower δD values than type II chondrule mesostases would then presumably be due to the difference in the diffusivities of $H_2O$ in glasses of different composition. However, type I chondrules can have higher $H_2O$ contents than some type II chondrules, which would suggest that secondary $H_2O$ enrichment of chondrule mesostases occurred through multiple mechanisms at different stages of $H_2$ loss from the parent bodies. Nonetheless, the D-enrichment process via $H_2$ loss through Fe metal oxidation may also explain the variable δD values observed in the chondrule mesostases of DOM 08006 (Fig. 6). The smaller amount of D-enrichment in DOM 08006 may be due to a smaller fractional H loss that was more similar to those of CM, CI, and CR chondrites (Sutton et al., 2017). Compared to Semarkona and DOM 08006, QUE 97008 experienced a greater degree of thermal metamorphism (Grossman and Brearley, 2005), which should have led to both a greater degree of H loss (and D enrichment) and more complete isotopic equilibration of the $H_2O$ in its chondrules. This is what we observe in QUE 97008 chondrules.

### 5.2. Primary HVE contents in chondrules

As shown in the previous section, there are several lines of evidence that favor the HVEs we have measured in the chondrules being largely secondary in origin. However, there are remaining issues with this secondary origin hypothesis that suggests that some of the HVEs in the chondrules are primary in origin.

#### *5.2.1. Phenocryst/melt partition coefficients of HVEs*

To evaluate whether or not any of the HVEs in the chondrule mesostases could be primary in origin, the partition coefficients of HVEs between chondrule phenocrysts and glasses can be compared to the igneous partition

coefficients determined by experimental studies (Fig. 10) (e.g., Hauri et al., 2006; Rosenthal et al., 2015). However, caution must be taken in making this comparison as most of the experimental partition coefficients were determined at significantly higher pressures and under more oxidizing conditions (e.g., 1 GPa and FMQ) compared to those that are generally assumed for chondrule formation. The ranges of $H_2O$ and Cl contents in the chondrule phenocrysts are fairly small (8–14 ppm and 0.04–0.07 ppm, respectively) relative to the ranges in the mesostases (8–10,200 ppm and 0.07–175 ppm, respectively), such that most of the variations in the observed partition coefficients are due to the variations in the $H_2O$ and Cl contents in the mesostases (Fig. 10a and b). This is also the case for partition coefficients for $CO_2$ (Fig. 10c), and to a lesser extent for S partition coefficients (Fig. 10d). Since the HVE contents in the mesostases tend to be enriched at the rims of the chondrules (Figs. 4, S5, and S6), the lowest partition coefficients are observed towards the rims of the chondrules. This is similar to what is observed for partitioning of Na between high-Ca pyroxene and mesostasis, which was interpreted to be the result of secondary addition of Na to the mesostases (Alexander and Grossman, 2005). However, on average, the phenocryst/glass partition coefficients of HVEs observed in the chondrules are higher than those determined experimentally, which is the opposite of the low partition coefficients that would be expected if the HVEs are secondary and were added to the mesostases after solidification. For example, the observed chondrule phenocryst/mesostasis partition coefficients for $H_2O$ and Cl range from 0.002 to 1.4 and 0.0004 to 0.1, respectively (Fig. 10a and b). The observed chondrule partition coefficients are, contrary to the secondary origin hypothesis of the $H_2O$ and Cl, mostly comparable to or higher than the experimentally determined partition coefficient ($H_2O$: 0.0015 for olivine/melt and 0.019 for low-Ca pyroxene/melt, Cl: 0.002 for olivine/melt and 0.0024 for low-Ca pyroxene/melt) (Hauri et al., 2006), with the exception of the most $H_2O$ and Cl enriched Semarkona chondrule mesostases in chondrule S1.

An alternative interpretation is that the high partition coefficients are primary igneous partition coefficients. The recent experiments of Sarafian et al. (2019) showed that $H_2O$ is significantly more compatible ($D_{H2O} = 0.1$) in low-Ca pyroxene at a low pressure of 0.1 MPa, $fO_2$ of ~FMQ, and a temperature of 1160 °C, which perhaps supports this interpretation. To our knowledge, such low-pressure experimental partitioning data is not available for Cl. Another possible interpretation is that, the mesostases with the highest $H_2O$ and Cl contents and lowest partition coefficients (i.e., most igneous-like partition coefficients) record the original mesostases $H_2O$ and Cl contents, and that the rest of the mesostases record $H_2O$ and Cl contents after partial $H_2O$ and Cl degassing. However, this seems unlikely as the parts of the chondrule mesostases that record the lowest

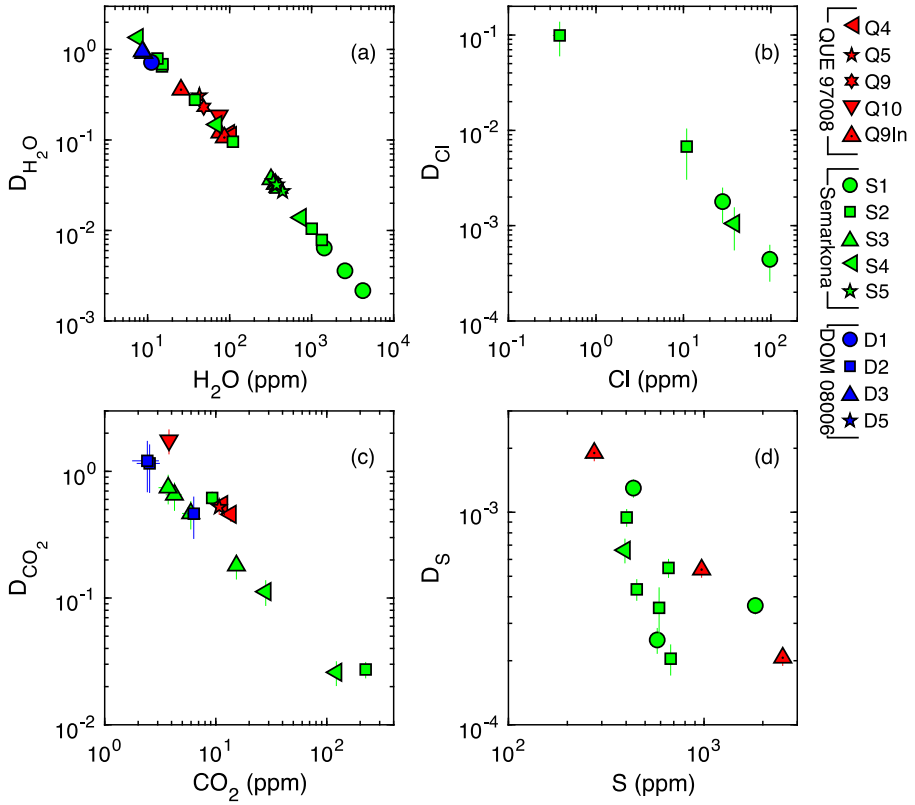


Fig. 10. The partition coefficients for (a) $H_2O$, (b) Cl, (c) $CO_2$, and (b) S between phenocrysts (olivine or orthopyroxene) and the adjacent mesostasis glasses in the chondrules of QUE 97008 (red), Semarkona (green), and DOM 08006 (blue). (For interpretation of the references to colour in this figure legend, the reader is referred to the web version of this article.)

partition coefficients (i.e., the highest $H_2O$ and Cl contents) are towards the rims of the chondrules (Fig. 4, Figs. S5 and S6). In addition, chondrule melt inclusions in chondrule S1 that probably record the more pristine $H_2O$ and Cl contents have $H_2O$ and Cl contents that are significantly lower than those in the chondrule mesostases (Fig. 4). Perhaps the most plausible explanation for the high partition coefficients we observe is that the $H_2O$ and Cl in the phenocrysts is also secondary and/or there are additional blank contributions to our measurements that we have not taken into account. For example, Deloule et al. (1998) found evidence of amphibole in low-Ca pyroxene phenocrysts in Bishunpur (LL3.15) chondrules. Although to our knowledge, it has not been observed in meteorite olivines, clinohumite has been observed in terrestrial olivines from the Zabargad peridotites, Red Sea (Mosenfelder et al., 2006). If these phases are present in the chondrule phenocrysts in our samples, they would compromise our $H_2O$ and Cl partition coefficient calculations for the low-Ca pyroxenes and olivines.

The observed olivine/melt partition coefficients for $CO_2$ range from 0.026 to 1.8 ($CO_2$ in the low-Ca pyroxenes were below the detection limits), and are also significantly higher than the experimental olivine/melt and low-Ca pyroxene/melt partition coefficients of $0.0007 \pm 0.0004$ and $0.0003 \pm 0.0002$, respectively (Rosenthal et al., 2015) (Fig. 10b). This is again seemingly inconsistent with the secondary origin hypothesis for C in the chondrule mesostases, which would predict the measured partition coefficients to be lower than the experimental ones. Given the relatively low $CO_2$ concentrations of 2.4–1170 ppm in the mesostases, the $CO_2$ in the phenocrysts should be undetectable (below our detection limit of 2 ppm) according to the experimental partition coefficients (Rosenthal et al., 2015). If the mesostases lost much of their original $CO_2$, but the phenocrysts did not, this would require an original $CO_2$ content of up to ~2 wt.% in the melt. While this would require a very high vapor pressure of $CO/CO_2$ if melt-gas equilibrium were assumed, it is difficult to rule out that mesostases had such a high $CO_2$ content due to the disequilibrium process of incomplete $CO/CO_2$ loss (Hanon et al., 1998 and Section 5.1.2). Again, however, relative enrichments in C contents in the mesostases occur at the chondrule edges at least in some chondrules (Figs. S5 and S6), which is inconsistent with the expectation for degassing that the highest C contents would occur in the chondrule cores. Hence, similar to $H_2O$, perhaps the most likely explanation for the high $CO_2$ partition coefficients we observe is that the $CO_2$ abundances in the olivine phenocrysts are secondary and/or we have underestimated the blank contributions. On the other hand, the phenocryst/melt partition coefficients for S are comparable to or slightly lower than the experimentally observed partition coefficients (Fig. 10d) (olivine/melt = 0.001 and low-Ca pyroxene/melt = 0.003 for S) (Hauri et al., 2006; Callegaro et al., 2020). While the lower partition coefficients may suggest some secondary influx of S into the mesostases, the similarity between some observed and experimental partition coefficients may suggest a primary origin of some of the S in the chondrule mesostases and the phenocrysts. Potential evidence of primary S in the mesostases is discussed in more detail in Section 5.2.4.

#### 5.2.2. Presence of HVEs in chondrule melt inclusions

While they are more HVE depleted than the chondrule mesostases, the melt inclusions analyzed in the Semarkona chondrule S1 contain measurable amounts of HVEs that are significantly above our detection limits (Fig. 4). This may be consistent with the HVEs in the melt inclusions being primary, and that they were protected to a large extent by the surrounding olivine from the secondary influx of HVEs into the chondrule mesostases. Previous studies have shown that olivine hosted melt inclusions do not act as a closed system at high temperature for $H_2O$ (e.g., Gaetani et al., 2012; Bucholz et al., 2013) due to the fast diffusion of H in olivine (e.g., Kohlstedt and Mackwell, 1998; Demouchy and Mackwell, 2006). In our case, however, temperatures in their parent bodies were low enough to slow the H diffusion through the olivine surrounding our melt inclusions, such that it acted as a protective shell against the secondary influx of HVEs into the melt inclusions. The $H_2O$ concentrations in the melt inclusions of 13 ppm to 18 ppm match well with those predicted (~10–20 ppm, Section 5.2.3 for details) for a chondrule silicate melt that formed at $10^3$ to $10^5 \times$ CI dust enrichment, relative to the solar composition, with an $f_{O2}$ of IW−1.2 to +0.5, and pressure of $10^{-3}$ bars (Ebel and Grossman, 2000; Fedkin and Grossman, 2013). If we use the method described in Section 5.1.2 for estimating the partial pressures of certain volatile species ($H_2$, $H_2O$, CO, and $CO_2$) in the gas phase from the $H_2O$ and $CO_2$ contents, the ranges in partial pressures of volatile species inferred from the melt inclusion compositions are $3.3 \times 10^{-4}$–$5.9 \times 10^{-4}$ bars for $H_2O$, 0.03–0.05 bars for $H_2$, 0.05–0.07 bars for $CO_2$, and 12–16 bars for CO. While the lower partial pressure estimates for $H_2O$ and $H_2$ are perhaps consistent with transient conditions in the nebula, the CO and to a lesser extent the $CO_2$ partial pressures are not. This could suggest that there is secondary C in the melt inclusions, but the melt inclusions should to have suffered minimal secondary influx of $H_2O$ that likely diffuses faster than C in olivine. Alternatively, the C content in the chondrule mesostases may not record the equilibrium solubility, but instead the disequilibrium process of incomplete CO loss from the chondrule mesostases (Hanon et al., 1998 and Section 5.1.2). Our results suggest that while there is the potential for the $H_2O$ in the melt inclusions to be primary in origin (discussed in more detail in Section 5.2.3), further work is required to assess the origin of the C in the melt inclusions. The origin of S in the melt inclusion as well as chondrule mesostases in general is discussed in Section 5.2.4. The assessment of the partial pressures of the halogens and, therefore, the assessment of the origin of F and Cl in the melt inclusions is out of the scope of the present study.

#### 5.2.3. Predicted $H_2O$ contents in chondrule melts under canonical formation conditions

The presence of small but measurable amounts of $H_2O$ (<18 ppm) in the melt inclusions of Semarkona chondrule S1 suggests that some of the $H_2O$ in the chondrules is

primary in origin. Several previous studies have hypothesized that significantly greater concentrations of $H_2O$ ($H_2$/OH/$H_2O$) than measured here in chondrule mesostases are primary (up to 8.7 wt.% and 1.2 wt.% by Stephant et al. (2017) and Piani et al. (2020), respectively). To have a better constraint on the concentration of primary $H_2O$ that may be dissolved in the mesostases during chondrule formation, we calculated the dissolved $H_2O$ content in a silicate melt under a range of pressure and $f_{O2}$ conditions that are relevant to chondrule formation.

In our calculations, we assume a gas composition that is composed of the species $H_2$ and $H_2O$ (i.e., $P_{H2} + P_{H2O} = P_{Total}$). These are the major of gas phase species in chondrule formation models that use a solar gas and CI dust compositions (e.g., Fedkin and Grossman, 2013). In these models, however, there are other species in the gas phase such as He and CO that dilute the $H_2$ and $H_2O$ in the gas. These other species comprise a relatively small molar fraction of the gas (17% to 27% depending on degree of CI dust enrichment, Fedkin and Grossman, 2013). Nevertheless, the total pressures in our calculations should be considered minimum values at a given $P_{H2}$, $P_{H2O}$, and $f_{O2}$ conditions. We first calculate the $f_{H2}/f_{H2O}$ ratio using the free energy of the reaction $H_2 + 0.5O_2 \Leftrightarrow H_2O$ using thermodynamic data from JANAF (Chase, 1998) assuming a temperature of 1300 °C and a range of $f_{O2}$ from IW−4 to IW +0.5. The range of $f_{O2}$ was chosen as it encompasses the expected $f_{O2}$ in CI dust enriched bulk compositions for $10^2$ to $10^5 \times$ CI dust enrichments, relative to the solar composition (e.g., Ebel and Grossman, 2000; Fedkin and Grossman, 2013). The $f_{H2}$ and $f_{H2O}$ are then calculated using the $f_{H2}/f_{H2O}$ ratio along with the equations of state of $H_2$ and $H_2O$ of Zhang and Duan (2009) at a range of pressure conditions ($10^{-4}$ to 100 bars). This range of pressures was chosen to cover the range predicted for those of chondrule formation from previous studies (e.g., Ebel and Grossman, 2000; Alexander et al., 2008; Fedkin and Grossman, 2013). Finally, the silicate melt solubility equations for $H_2$ (eq. 6 of Hirschmann et al., 2012) and $H_2O$ (eq. 7 of Newcombe et al., 2017) were used to calculate the $H_2$ and $H_2O$ contents in the melt. Equation 7 of Newcombe et al. (2017) is applicable under conditions where most of the $H_2O$ is dissolved in the melt as hydroxyl, which is a valid assumption for the low total $H_2O$ dissolved in the melts in our calculations.

The calculated total $H_2O$ solubility ($H_2$ (calculated as $H_2O$) + $H_2O$) in the melt ranges from 0.8 ppm ($10^{-4}$ bar, IW−4) to ~6000 ppm (100 bars, IW + 0.5) (Fig. 11). The contribution of $H_2$ to the $H_2O_{tot}$ by weight ranges from <1% (<$10^{-1}$ bar, all $f_{O2}$) to 29% (100 bars, IW−4). The highest calculated $H_2O_{tot}$ content in the melt (~6000 ppm), suggests that a large amount of $H_2O$ could be dissolved in chondrule melts if they were generated under the most extreme conditions that have been proposed by previous studies. A more conventional total pressure of $10^{-3}$ bars would result in chondrule melts having between ~10 ppm ($10^3 \times$ CI dust enrichment and $fO_2$ of IW−1.2, Ebel and Grossman, 2000) and ~20 ppm $H_2O_{tot}$ ($10^5 \times$ CI dust enrichment and $fO_2$ of IW + 0.5, Fedkin and Grossman, 2013). The calculated $H_2O$ content at

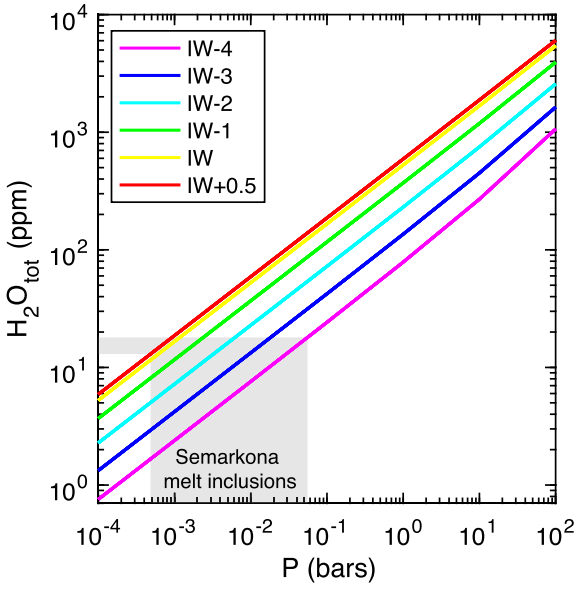


Fig. 11. Calculated total $H_2O$ solubility ($H_2$ (calculated as $H_2O$) + $H_2O$) in silicate melt in equilibrium with $H_2$ and $H_2O$ gas at a range of total pressures and $f_{O2}$ conditions. Refer to Section 5.2.3 for the details of the calculations. The gray field indicates the range in the $H_2O$ content (13–18 ppm) in the melt inclusions in Semarkona chondrule S1 (Section 5.1.3), and the corresponding range in total pressure at $H_2O$ saturation (0.0005–0.055 bars).

$H_2O$ saturation in the silicate melt as a function of pressure and $f_{O2}$ can be used to estimate the range of total pressures at which the melt inclusions in Semarkona chondrule S1 (Section 5.1.3) would have had to be generated. To dissolve the measured $H_2O$ contents, 13–18 ppm $H_2O$, in a silicate melt requires total pressures ($P_{H2} + P_{H2O}$) of 0.0005–0.029 bars and 0.0009–0.055 bars (depending on the $f_{O2}$), respectively (Fig. 11). These ranges overlap with previously estimated nebular pressures during chondrule formation (Alexander, 2004; Cuzzi and Alexander, 2006), suggesting that the $H_2O$ we measured in the melt inclusions could be of primary origin.

The recent study of Piani et al. (2020) reported $H_2O$ contents of 2700–12,300 ppm $H_2O$ in the chondrule mesostases of SAH 97096 (EH3.1-3.4). To dissolve such high $H_2O$ contents in the silicate melt requires ranges in pressure of 20–380 bars and 400–2350 bars (depending on the $f_{O2}$), respectively (Fig. 11). Given the highly reduced nature of most enstatite chondrite chondrules, the highest pressures in these ranges seem more appropriate. Piani et al. (2020) argued that the $H_2O$ contents measured in their chondrule mesostases must have been acquired before parent body formation, possibly during chondrule formation, on the basis of the lack of aqueous alteration signatures in SAH 97096. However, our study has shown that the chondrule mesostases of Semarkona that do not show overt signs of aqueous alteration but contain up to ~10,200 ppm of $H_2O$ have most likely been hydrated during parent body processes (Section 5.1.3). Given the extreme pressure conditions required to dissolve 2700–12,300 ppm $H_2O$ in a silicate melt, the $H_2O$ measured in the chondrule mesostases

of SAH 97096 by Piani et al. (2020) are more likely to be secondary and/or due to terrestrial contamination.

This is even more likely to be the case for the study of Stephant et al. (2017) that reported even higher $H_2O$ contents in chondrule mesostases (2300 ppm to 8.7 wt.%) from Paris (CM2), Renazzo (CR2), and Bishunpur (LL3.15). As did the Piani et al. (2020) study, these authors argued that the $H_2O$ contents they measured in the chondrules were acquired during chondrule formation and not in the parent body. To retain the high $H_2O$ contents of between 2300 ppm and 8.7 wt.% in a silicate melt would require extraordinary pressure conditions of 13–300 bars to 8000–12,000 bars (depending on the $f_{O2}$, calculated using the method described earlier in this section), respectively. The study of Stephant et al. (2017) also reported high $H_2O$ contents in chondrule olivines (76–1051 ppm) and pyroxenes (266–1796 ppm), which would suggest the equilibrium silicate melts had $H_2O$ contents of 5–70 wt.% and 1.4–9.5 wt.%, respectively ($H_2O$ partition coefficients for olivine/melt = 0.0015 and for low-Ca pyroxene/melt = 0.019; Hauri et al., 2006). These are unrealistic $H_2O$ contents that would require extraordinary pressure conditions. Hence, the high $H_2O$ contents in chondrule mesostases, olivines, and pyroxenes reported by Stephant et al. (2017) are also likely to be secondary and/or due to terrestrial contamination.

*5.2.4. Evidences for primary alkali and sulfur in chondrules*

While much of the Na in mesostases in the zoned regions of Semarkona chondrules is likely secondary in origin, it has been argued that the Na in the chondrule cores is largely primary (Alexander and Grossman, 2005; Alexander et al., 2008). Although there is a considerable amount of scatter, the Na contents of the high-Ca pyroxene and glass at the cores of type I and II chondrules in our study are roughly consistent with igneous partitioning of Na (Alexander and Grossman, 2005) (Fig. 12). Similar to Na, the sulfides as well as S in chondrule mesostases have also been argued to be either primary and/or secondary in origin (e.g., Blum et al., 1989; Zanda et al., 1995; Krot et al., 1997; Rubin et al., 1999; Marrocchi and Libourel, 2013; Piani et al., 2016). Secondary sulfides have been argued to form through thermal metamorphism (Blum et al., 1989; Zanda et al., 1995), shock metamorphism (Rubin, 1992), hydrothermal alteration (Krot et al., 2004), and metal-gas reaction (Lauretta et al., 1997). These secondary sulfides include those that have veins that connect to sulfides at the chondrule rims (Rubin, 1992) or are associated with magnetite and carbide (Krot et al., 1997). However, sulfides that are in the chondrule interiors and are not associated with such features have been argued to be primary in origin (Rubin et al., 1999; Tachibana and Huss, 2005). Primary sulfide melts should be rapidly lost at chondrule formation temperatures and low pressures (Hewins and Connolly, 1996; Hewins et al., 1997; Hewins et al., 2005). Yet, the S isotopic compositions of chondrule sulfides do not show evidence of significant isotopic fractionation that would be expected from free evaporation (Tachibana and Huss, 2005). This suggests that the evaporation of S from chondrule melts was suppressed (Marrocchi and Libourel, 2013), and this requires high partial pressures of S during chondrule formation. In addition to the petrologic and S isotopic evidence, the correlated behavior of FeO and S contents in chondrule mesostases have been argued to be consistent with those predicted by models of sulfide saturation, and this has been argued to be evidence for the igneous origin of S in chondrule mesostases (Marrocchi and Libourel, 2013; Piani et al., 2016).

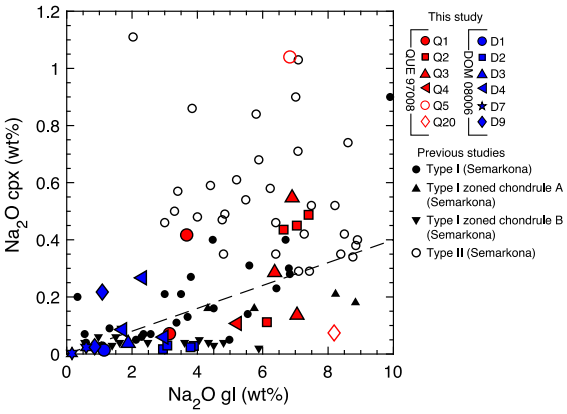


Fig. 12. $Na_2O$ contents in high-Ca pyroxenes (cpx) versus the $Na_2O$ contents in the adjacent chondrule mesostases (gl) of QUE 97008 (red) and DOM 08006 (blue). The filled symbols are from type I chondrules, and the open symbols are from type II chondrules. There are cpx both as overgrowths and small phenocrysts in Semarkona chondrules, but they were not measured here as they have been studied by others. The black filled circles are data on type I chondrules in Semarkona from previous studies (Jones and Scott, 1989; Jones, 1994; Alexander and Grossman, 2005). The black filled triangles and inverted triangles are zoned Semarkona chondrules A and B, respectively, from Alexander and Grossman (2005). The open circles are data from type II Semarkona chondrules from previous studies (Jones, 1990, 1996; Alexander and Grossman, 2005). The dashed line is the experimentally determined partition coefficient for the albite-diopside system (Blundy et al., 1995). (For interpretation of the references to colour in this figure legend, the reader is referred to the web version of this article.)

To evaluate whether the chondrule mesostases in our study were sulfide-saturated towards the end of crystallization, we have used the sulfide saturation model of Smythe et al. (2017). We assumed a temperature of 1050 °C, a pressure of $10^{-3}$ bars, and that troilite is the stable sulfide. The temperature was chosen to be the temperature of crystallization of the last phase to crystallize in the chondrule – i.e., high-Ca pyroxene, and the pressure was chosen based on previous studies of chondrule formation (Alexander, 2004; Cuzzi and Alexander, 2006) and our pressure estimates in Section 5.2.3. The calculated S content at sulfide saturation (SCSS) is significantly higher for the type I chondrule mesostases relative to those in type IIs (Fig. 13a). This is because SCSS is predicted to increase with decreasing FeO content in the melt (Mavrogenes and O'Neill, 1999; Smythe et al., 2017). The calculated SCSS agrees reasonably well with the measured S contents in the type II chondrule mesostases (Fig. 13b), suggesting that they were likely

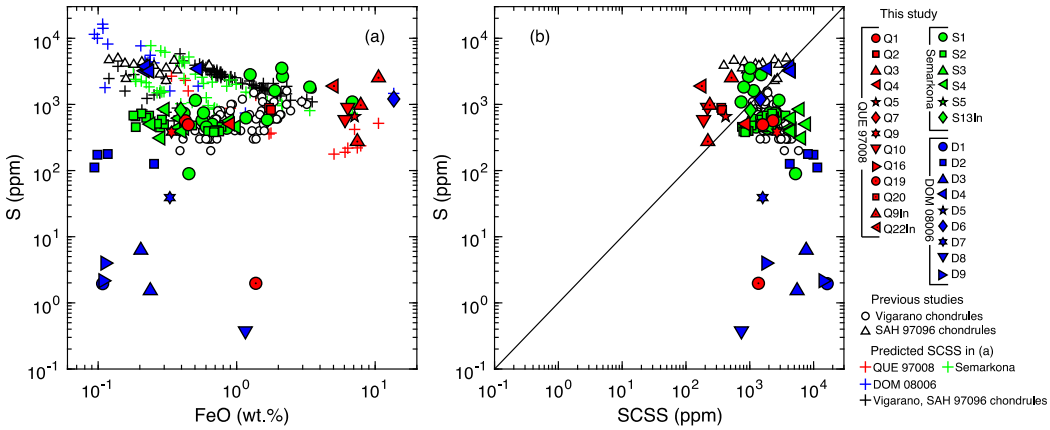


Fig. 13. (a) The S versus FeO contents, and versus (b) the predicted S contents at sulfide saturation (SCSS) of the chondrule mesostases in QUE 97008 (red), Semarkona (green), and DOM 08006 (blue). The white circles are for the Vigarano (CV3) chondrules from Marrocchi and Libourel (2013) and white triangles are for the SAH 97096 (EH3) chondrules from Piani et al. (2016). The plus signs in (a) are the SCSS of the chondrule mesostases predicted using the model of Smythe et al. (2017) that is detailed in Section 5.2.4. (For interpretation of the references to colour in this figure legend, the reader is referred to the web version of this article.)

sulfide-saturated. This is consistent with the observation of sulfides in our type II chondrules, which are likely primary in origin as they are located in the chondrule interiors and are not associated with either veins (Rubin, 1992) or magnetite and carbide (Krot et al., 1997).

In contrast to the type II chondrule mesostases, the calculated SCSS is significantly higher than the measured S contents in type I chondrule mesostases (with the exception of chondrule #4 in DOM 08006) (Fig. 13b). This would suggest that type I chondrule mesostases were sulfide undersaturated at the time of solidification. However, inspection of some of our type I chondrules under the SEM shows that there are small sulfides grains in the mesostases (e.g., DOM 08006 chondrule D4), despite being significantly less abundant than in type II chondrules. Further, there are experimental results, such as those of Liu et al. (2007), Ariskin et al. (2013), and Fortin et al. (2015), that, contrary to model predictions, show that some low FeO (i.e., $< 1$ wt.%) silicate melts can have relatively low SCSS (~100–600 ppm). Hence, the compositions of the low FeO type I chondrule mesostases could be outside of the compositional range used in developing the model of Smythe et al. (2017), and at least some of our type I chondrule mesostases were sulfide saturated at the time of solidification.

### 5.2.5. Upper limits of primary HVE contents of bulk silicate chondrules

Here we use our analyses of chondrule mesostases and phenocrysts that we judge to be the least modified by secondary processes to estimate the upper limits of the abundances of primary HVEs in the silicate portions of the type I and II chondrules. We report our estimates as upper limits because it is difficult to rule out the potential effects of secondary modification and contamination on the HVE contents. To minimize the influence of these effects, we chose the chondrules that are representative of those with the lowest HVE contents that we have measured in this study. We argue that this is justified by the fact that the melt inclusions in the Semarkona chondrule S1, which are protected to a large extent from the secondary influx of HVEs by the surrounding olivine, record significantly lower HVE contents than the mesostases (Section 5.1.3). We used the analyses of chondrules in Semarkona and DOM 08006 rather than those of QUE 97008 given the greater thermal metamorphism QUE 97008 experienced (Section 5.1.5).

We chose the analyses of chondrules S2 (S2-4-a) and D1 (D1-1) as upper limits for primary HVE contents in the silicate portions of type I chondrules in Semarkona and DOM 08006, respectively. For the type II chondrules of Semarkona and DOM 08006, we chose the analyses of chondrules S3 (S3-1) and D6 (D6-1), respectively. The bulk silicate compositions of these chondrules were estimated using

Table 2
Upper limits of volatile contents of the silicate portion of type I and II chondrules.

| Chondrule type | Type I | | Type II | |
|---|---|---|---|---|
| Chondrule | S2 | D1 | S3 | D6 |
| $H_2O$ (ppm) | 11 | 7 | 85 | 50 |
| $CO_2$ (ppm) | 0.6[a] | 0.3 | 3 | 0.4[a] |
| Cl (ppm) | 0.03 | 0.01 | 2 | 0.04 |
| S (ppm) | 60 | 0.3 | 190 | 260 |
| F (ppm) | 0.2 | 0.1 | 2 | 0.04[a] |
| $H/Al_{CI}$[b] | $2.3 \times 10^{-5}$ | $1.2 \times 10^{-5}$ | $3.5 \times 10^{-4}$ | $2.2 \times 10^{-4}$ |
| $C/Al_{CI}$[b] | $1.6 \times 10^{-6}$ | $0.8 \times 10^{-6}$ | $1.8 \times 10^{-5}$ | $2.4 \times 10^{-6}$ |
| $Cl/Al_{CI}$[b] | $1.6 \times 10^{-5}$ | $4.0 \times 10^{-6}$ | $1.6 \times 10^{-3}$ | $3.6 \times 10^{-5}$ |
| $S/Al_{CI}$[b] | $3.9 \times 10^{-4}$ | $1.5 \times 10^{-6}$ | $2.5 \times 10^{-3}$ | $3.5 \times 10^{-3}$ |
| $F/Al_{CI}$[b] | $1.0 \times 10^{-3}$ | $5.2 \times 10^{-4}$ | $2.3 \times 10^{-2}$ | $5.3 \times 10^{-4}$ |

[a] The detection limits were used to calculate these upper limit concentrations as the measured concentrations were below our detection limits.

[b] The ratios are normalized to the CI ratios from Palme et al. (2014).

the compositions and modal abundances of mesostases and phenocrysts. The modal abundances were estimated using SEM images of the chondrules (modal abundance of mesostases ranges from 14 vol.% to 30 vol.%), and we assumed equal densities of mesostasis and phenocryst for simplicity. While this is a simplified approach, the $Mg/Si_{CI}$ and $Al/Si_{CI}$ ratios (normalized to CI) of our estimated bulk silicate chondrule compositions are consistent with the previously observed ranges in their chondrule types (type IA: chondrules S2 and D1, type IIA: chondrule S3, and type IIB: chondrule D6) (Jones and Scott, 1989; Jones, 1990, 1994, 1996) (Fig. S11).

The upper limits of the HVEs in the silicate portion of type I and II chondrules (in ppm of $CO_2$, $H_2O$, Cl, S, and F and in $C/Al_{CI}$, $H/Al_{CI}$, $Cl/Al_{CI}$, $S/Al_{CI}$, and $F/Al_{CI}$ ratios (CI composition from Palme et al., 2014) are listed in Table 2. The HVEs are extremely depleted relative to the refractory elements as expected from the high temperatures and low pressures typically assumed for chondrule formation condition(s). When plotted as a function of the 50% condensation temperatures ($T_c$) at a pressure of $10^{-4}$ bars (Wood et al., 2019) (Fig. 14a and b), the Al- and CI-normalized concentrations of HVEs in the chondrules generally decreases with decreasing $T_c$. In both Semarkona and DOM 08006, the type I chondrules are more depleted in HVE contents than type II chondrules. The concentration of HVEs in both type I and II chondrules of Semarkona decrease relatively smoothly with decreasing $T_c$. In contrast, HVE concentrations in both type I and II chondrules of DOM 08006 show a more irregular decrease with decreasing $T_c$. In particular, Cl in both type I and II DOM 08006 chondrules are lower compared to those of Semarkona, and S is significantly lower in the type I DOM 08006 chondrules than in those in Semarkona. While more work is required to better constrain the cause of such differences between the Semarkona and DOM 08006 chondrules, it could be due to: (1) greater secondary influxes of Cl and S into the Semarkona chondrules compared to those

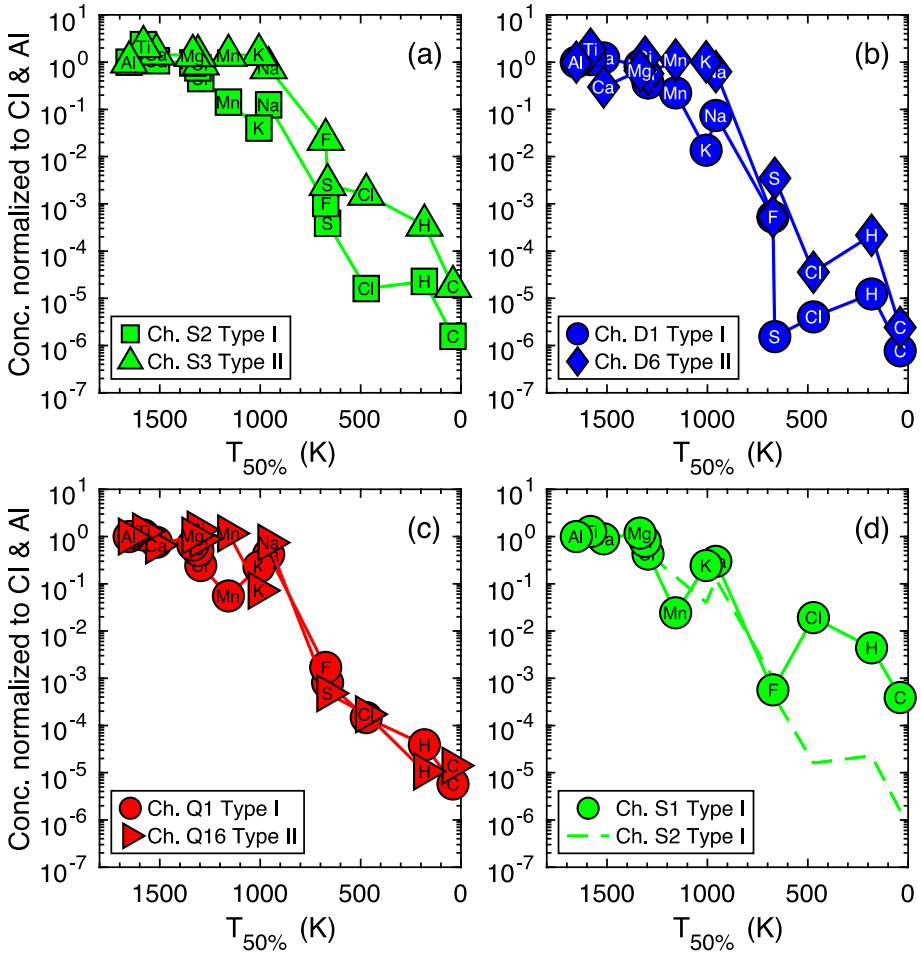


Fig. 14. Elemental concentrations in the silicate portions of chondrules normalized to Al and CI (Palme et al., 2014) plotted as a function of their 50% condensation temepratures ($T_c$) (Wood et al., 2019) (siderophile elements Fe, Ni, and P were excluded for clarity). Panels (a) and (b) show Semarkona and DOM 08006 chondrules, respectively, that are least modified by secondary processes. Carbon concentrations in chondrules S2 (a) and chondrule D6 (b), and the F concentration in chondrule D6 are below our detection limits, so the detection limits of C and F are used as the upper limits. Panels (c) and (d) show QUE 97008 and Semarkona (S1) chondrules, respectively, that are most likely modified by secondary processes. In (d), the least modified type I Semarkona chondrule (S2) is also shown for comparison. Refer to Section 5.2.5 for the specific analysis of each chondrules that were used.

of DOM 08006, (2) differences in the chondrule precursor compositions, with the DOM 08006 chondrule precursor material being more depleted in Cl and S relative to those of Semarkona, or (3) differing formation conditions for Semarkona and DOM 08006 chondrules.

We also present examples of Semarkona and QUE 97008 chondrules that show evidence for secondary modification of HVEs as compared to the pristine chondrules. For example, in QUE 97008 that experienced a greater degree of thermal metamorphism, the most HVE depleted type I (Q1-1) and II (Q16) chondrules do not show significant differences between their HVE concentrations (Fig. 14c). This is in contrast to the aforementioned differences in the HVE concentrations between type I and II chondrules of Semarkona and DOM 08006 (Fig. 14a and b). This would suggest that the greater thermal metamorphism experienced by QUE 97008 homogenized the HVE concentrations between the type I and II chondrules, consistent with their homogeneous δD values (Section 5.1.5). Another example is the Semarkona chondrule S1 (S1-t13) that shows significant evidence of secondary influx of HVEs (Fig. 14d). This chondrule is generally enriched in most of the HVEs (except for F) compared to the more pristine Semarkona chondrules, and it is particularly enriched in H and Cl that show evidence of secondary influx coupled with FeO (Section 5.1.3, Fig. 5a and b). This combined influx of H and Cl with Fe is not observed in the QUE 97008 and DOM 08006 chondrules, and it is consistent with the evidence for more extensive aqueous alteration in Semarkona compared to QUE 97008 and DOM 08006 (Section 5.1.3).

In summary, our results suggest that (1) thermal metamorphism resulted in homogenization of the HVEs in type I and II chondrules, and that (2) aqueous alteration resulted in the anomalous enrichment of HVEs in chondrules, particularly in H and Cl. While we attempted to minimize such effects, we cannot completely rule out that they affected the estimated upper limits of the HVEs in the silicate portion of type I and II chondrules (Table 1 and Fig. 14a and b). Nonetheless, we use these upper limit HVE contents to estimate the upper limits of the partial pressures of $H_2O$, $H_2$, $CO_2$, and CO in the gas during chondrule formation (refer to Section 5.1.2 for calculation methods). These upper limits for the type I chondrules are: $1.0 \times 10^{-4}$ to $2.4 \times 10^{-4}$ bars for $H_2O$, 0.007–0.012 bars for $H_2$, 0.006–0.009 bars for $CO_2$, and 1.0–1.4 bars for CO. The upper limits for the type II chondrules are, 0.005–0.014 bars for $H_2O$, 0.012–0.052 bars for $H_2$, 0.17–0.28 bars for $CO_2$, and 1.1–3.2 bars for CO. For improved constraints on the chondrule formation conditions as well as the behavior of HVEs during chondrule formation, further efforts are required to improve the understanding of secondary influx of HVEs into the chondrules during parent body processes.

## 6. CONCLUSIONS

We performed high spatial resolution and low background SIMS analyses of the H, C, F, Cl, and S concentrations and H isotopic compositions in type I and II chondrules in the primitive ordinary chondrites Semarkona (LL3.00) and QUE 97008 (L3.05), and the primitive carbonaceous chondrite DOM 08006 (CO3.00). HVE contents and H isotopic compositions in the chondrule mesostases vary significantly ($H_2O$: 8–10,200 ppm, $CO_2$: 2.4–1170 ppm, F: 0.3–30 ppm, Cl: 0.07–175 ppm, S: 0.38–4400 ppm, δD: 77–15,000‰). Phenocrysts have, on average, lower HVE contents ($H_2O$: 8–14 ppm, $CO_2$: 2.8–7 ppm, F: <0.2 ppm, Cl: 0.04–0.07 ppm ppm, S: 0.14–0.7 ppm).

The predicted total pressures of gases in equilibrium with the mesostasis melts are mostly within $10^{-2}$–$10^{1}$ bars but are up to ~1900 bars, which are significantly higher than $\sim 10^{-3}$ bars expected for chondrule formation through nebular mechanisms. Although the predicted very large pressures could be reached, at least briefly, during planetesimal impacts, the predicted equilibrium compositions of the gases in impact-generated atmospheres ($H_2$, $H_2O$, CO and $CO_2$ in similar proportions) are very different from the estimated compositions from our chondrule mesostasis.

Enrichments in volatile contents in mesostasis close to the edge of chondrules, positive correlations between FeO and $H_2O$ and Cl, and depletions (compared to mesostasis) in $H_2O$ and Cl in melt inclusions in olivine phenocrysts suggest strong secondary influxes of volatiles from the surrounding matrix material into the chondrule mesostases. The fact that the estimated diffusion distances of $H_2O$ in silicate glasses (300 °C, 1 Myr duration of alteration/metamorphism) are comparable to or greater than the radii of the chondrules in our study lends plausibility to the secondary origin of $H_2O$ in the chondrule mesostases.

The extremely high δD values in the ordinary chondrite chondrules mesostases may be due to isotopic Rayleigh fractionation as a result of the loss of very D-poor $H_2$ generated by Fe metal oxidation by $H_2O$ ($3Fe + 4H_2O \Leftrightarrow Fe_3O_4 + 4H_2$) during alteration in the parent body. The D-rich water may have diffused into the chondrule mesostases.

The measurable concentrations of volatiles in the melt inclusions in olivine suggest that a small portion of volatiles in chondrules is primary in origin. Our estimates of contents of primary volatiles in the silicate portion of our type I and II chondrules that were the least affected by secondary influx of volatiles are: 1) 7–11 ppm $H_2O$, 0.3–0.6 ppm $CO_2$, 0.1–0.2 ppm F, 0.01–0.03 ppm Cl, and 0.3–60 ppm S in type I chondrules, and 2) 50–85 ppm $H_2O$, 0.4–3 ppm $CO_2$, 0.04–2 ppm F, 0.04–2 ppm Cl, and 190–260 ppm S in type II chondrules.

Using volatile contents in the silicate portion of chondrules studied in this work we have estimated the upper limits of partial pressures of $H_2O$, $H_2$, $CO_2$, and CO in the gas during chondrule formation: 1) in type I chondrules: $P_{H2O} = 1.0 \times 10^{-4}$ to $2.4 \times 10^{-4}$ bars, $P_{H2} = 0.007$–$0.012$ bars, $P_{CO2} = 0.006$–$0.009$ bars, and $P_{CO} = 1.0$–$1.4$ bars; 2) type II chondrules: $P_{H2O} = 0.005$–$0.014$ bars, $P_{H2} = 0.012$–$0.052$ bars, $P_{CO2} = 0.17$–$0.28$ bars, and $P_{CO} = 1.1$–$3.2$ bars.

## Declaration of Competing Interest

The authors declare that they have no known competing financial interests or personal relationships that could have appeared to influence the work reported in this paper.

## ACKNOWLEDGEMENTS

For supplying the sections of DOM 08006 and QUE 97008, the authors would like to thank: the members of the Meteorite Working Group, Cecilia Satterwhite and Kevin Righter (NASA, Johnson Space Center). US Antarctic meteorite samples are recovered by the Antarctic Search for Meteorites (ANSMET) program, which has been funded by NSF and NASA, and characterized and curated by the Department of Mineral Sciences of the Smithsonian Institution and Astromaterials Curation Office at NASA Johnson Space Center. For providing the section of Semarkona, the authors would like to thank Tim McCoy and Cari Corrigan of the Smithsonian Institution's National Museum of Natural History. Thoughtful and constructive reviews by three anonymous reviewers helped significantly improve this manuscript. KS and CA were supported by NASA Emerging Worlds grant 80NSSC18K0604.

## APPENDIX A. DETERMINING THE H, C, F, AND S BACKGROUNDS USING SUPRASIL GLASS IN MOUNT

As briefly discussed in Section 3.2, one could argue that H, C, F, and S backgrounds that are constrained using Suprasil glass mounted in In potentially underestimate those in the epoxy-bearing thin sections. Alternatively, chondrule phenocrysts (olivine/orthopyroxene) in the thin sections could provide more accurate backgrounds, if they are HVE-free. We have chosen the chondrule phenocryst analyses with ion images that show the least potential evidence of contamination due to overlap with mesostases as well as surface contamination and compared their HVE concentrations to those from the analyses of the Suprasil glass.

Comparisons of HVEs in the chondrule phenocrysts to those in Suprasil in a representative session (analytical session of the DOM 08006 section) show that F concentrations in the chondrule phenocrysts in the thin sections are very similar to those in the Suprasil (Fig. S2). This supports the use of Suprasil to determine the F background in the thin section. For C and S, the minimum C and S contents observed in the chondrule phenocrysts overlap with those in Suprasil. There are several analyses with higher concentrations in the chondrule phenocrysts (Fig. S2). Given the minimal evidence of surface contamination in these analyses, this would suggest that this is indigenous C and S. Alternatively, this may be due to contamination of the chondrule phenocryst ion images from the mesostases or undetected cracks that have higher C and S concentrations, despite the effort to minimize such effects. Given that the minimum measured C and S contents in chondrule phenocrysts overlap with those in Suprasil, as well as the potential for contamination and indigenous HVEs, we argue that analyses of Suprasil glass can provide more accurate F, C, and S backgrounds in the thin sections than chondrule phenocrysts.

The chondrule phenocrysts generally show higher concentrations of H relative to Suprasil (Fig. S2). The H results are unlike those for C or S in that nearly all measured H concentrations in chondrule phenocrysts are higher than those measured in Suprasil. If the higher H concentrations in the chondrule phenocrysts, relative to Suprail in the adjacent In mount, are solely due to the higher H background in the epoxy-bearing sections, no such difference should be observed if chondrule phenocrysts were mounted in the same In mount as Suprasil. We have compared the HVE concentrations measured in chondrule phenocrysts and Suprasil that were in the same In mount. Fig. S3 shows that the H concentrations are higher in the chondrule phenocrysts than that of Suprasil even in such case. Hence, we argue that this suggests that chondrule phenocrysts on average have higher inherent H concentrations than Suprasil, and that they are not completely "dry" material. Therefore, use of the H concentration in chondrule phenocrysts would likely overestimate the H background, and we argue that Suprasil glass provides a more accurate determination of the H background. Based on these observations, we have used the analyses of H, C, F, and S in Suprasil glass mounted in In (in the same holder as the thin section) to determine the backgrounds.

## APPENDIX B. SUPPLEMENTARY MATERIAL

Supplementary data to this article can be found online at https://doi.org/10.1016/j.gca.2021.03.005.

## REFERENCES

Alexander C. M. O'D., McKeegan K. D. and Altwegg K. (2018a) Water reservoirs in small planetary bodies: meteorites, asteroids, and comets. *Space Sci. Rev.* **214**, 36.

Alexander C. M. O'D., Newsome S. D., Fogel M. L., Nittler L. R., Busemann H. and Cody G. D. (2010) Deuterium enrichments in chondritic macromolecular material—Implications for the origin and evolution of organics, water and asteroids. *Geochim. Cosmochim. Acta* **74**, 4417–4437.

Alexander C. M. O'D. (1995) Trace element contents of chondrule rims and interchondrule matrix in ordinary chondrites. *Geochim. Cosmochim. Acta* **59**, 3247–3266.

Alexander C. M. O'D. (2004) Chemical equilibrium and kinetic constraints for chondrule and CAI formation conditions. *Geochim. Cosmochim. Acta* **68**, 3943–3969.

Alexander C. M. O'D. (2005) Re-examining the role of chondrules in producing the elemental fractionations in chondrites. *Meteorit. Planet. Sci.* **40**, 943–965.

Alexander C. M. O'D. (2019a) Quantitative models for the elemental and isotopic fractionations in chondrites: The carbonaceous chondrites. *Geochim. Cosmochim. Acta* **254**, 277–309.

Alexander C. M. O'D. (2019b) Quantitative models for the elemental and isotopic fractionations in the chondrites: The non-carbonaceous chondrites. *Geochim. Cosmochim. Acta* **254**, 246–276.

Alexander C. M. O'D., Barber D. J. and Hutchison R. (1989) The microstructure of Semarkona and Bishunpur. *Geochim. Cosmochim. Acta* **53**, 3045–3057.

Alexander C. M. O'D., Bowden R., Fogel M. L., Howard K. T., Herd C. D. K. and Nittler L. R. (2012) The provenances of asteroids, and their contributions to the volatile inventories of the terrestrial planets. *Science* **337**, 721–723.

Alexander C. M. O'D., Greenwood R. C., Bowden R., Gibson J. M., Howard K. T. and Franchi I. A. (2018b) A mutli-technique

search for the most primitive CO chondrites. *Geochim. Cosmochim. Acta* **221**, 406–420.
Alexander C. M. O'D. and Grossman J. N. (2005) Alkali elemental and potassium isotopic compositions of Semarkona chondrules. *Meteorit. Planet. Sci.* **40**, 541–556.
Alexander C. M. O'D., Grossman J. N., Ebel D. S. and Ciesla F. J. (2008) The formation conditions of chondrules and chondrites. *Science* **320**, 1617–1619.
Anders E. (1964) Origin, age, and composition of meteorites. *Space Sci. Rev.* **3**, 583–714.
Ariskin A. A., Danyushevsky L. V., Bychkov K. A., McNeill A. W., Barmina G. S. and Nikolaev G. S. (2013) Modeling solubility of Fe-Ni sulfides in basaltic magmas: the effect of nickel. *Econ. Geol.* **108**, 1983–2003.
Armstrong L. S., Hirschmann M. M., Stanley B. D., Falksen E. G. and Jacobsen S. D. (2015) Speciation and solubility of reduced C-O–H–N volatiles in mafic melt: Implications for volcanism, atmospheric evolution, and deep volatile cycles in the terrestrial planets. *Geochim. Cosmochim. Acta* **171**, 283–302.
Behrens H., Zhang Y., Leschik M., Wiedenbeck M., Heide G. and Frischat G. H. (2007) Molecular H2O as carrier for oxygen diffusion in hydrous silicate melts. *Earth Planet. Sci. Lett.* **254**, 69–76.
Bell D. R., Rossman G. R. and Moore R. O. (2004) Abundance and partitioning of OH in a high-pressure magmatic system: megacrysts from the Monastery kimberlite, South Africa. *J. Petrol.* **45**, 1539–1564.
Blum J. D., Wasserburg G., Hutcheon I. D., Beckett J. R. and Stolper E. M. (1989) Origin of opaque assemblages in C3V meteorites: Implications for nebular and planetary processes. *Geochim. Cosmochim. Acta* **53**, 543–556.
Blundy J. D., Falloon T. J., Wood B. J. and Dalton J. A. (1995) Sodium partitioning between clinopyroxene and silicate melts. *J. Geophys. Res.* **100**, 15501–15515.
Bollard J., Kawasaki N., Sakamoto N., Olsen M., Itoh S., Larsen K., Wielandt D., Schiller M., Connelly J. N. and Yurimoto H. (2019) Combined U-corrected Pb-Pb dating and 26Al-26Mg systematics of individual chondrules–Evidence for a reduced initial abundance of 26Al amongst inner Solar System chondrules. *Geochim. Cosmochim. Acta* **260**, 62–83.
Bonal L., Alexander C. M. O'D., Huss G. R., Nagashima K., Quirico E. and Beck P. (2013) Hydrogen isotopic composition of the water in CR chondrites. *Geochim. Cosmochim. Acta* **106**, 111–133.
Bonal L., Quirico E., Flandinet L. and Montagnac G. (2016) Thermal history of type 3 chondrites from the Antarctic meteorite collection determined by Raman spectroscopy of their polyaromatic carbonaceous matter. *Geochim. Cosmochim. Acta* **189**, 312–337.
Braukmüller N., Wombacher F., Hezel D. C., Escoube R. and Münker C. (2018) The chemical composition of carbonaceous chondrites: Implications for volatile element depletion, complementarity and alteration. *Geochim. Cosmochim. Acta* **239**, 17–48.
Bucholz C. E., Gaetani G. A., Behn M. D. and Shimizu N. (2013) Post-entrapment modification of volatiles and oxygen fugacity in olivine-hosted melt inclusions. *Earth Planet. Sci. Lett.* **374**, 145–155.
Budde G., Burkhardt C., Brennecka G. A., Fischer-Gödde M., Kruijer T. S. and Kleine T. (2016) Molybdenum isotopic evidence for the origin of chondrules and a distinct genetic heritage of carbonaceous and non-carbonaceous meteorites. *Earth Planet. Sci. Lett.* **454**, 293–303.
Busemann H., Alexander C. M. O'D. and Nittler L. R. (2007) Characterization of insoluble organic matter in primitive meteorites by microRaman spectroscopy. *Meteorit. Planet. Sci.* **42**, 1387–1416.
Callegaro S., Geraki K., Marzoli A., De Min A., Maneta V. and Baker D. R. (2020) The quintet completed: The partitioning of sulfur between nominally volatile-free minerals and silicate melts. *Am. Mineral.* **105**, 697–707.
Cassen P. (1996) Models for the fractionation of moderately volatile elements in the solar nebula. *Meteorit. Planet. Sci.* **31**, 793–806.
Chase, Jr., M. W. (1998) NIST-JANAF thermochemical tables. *J. Phys. Chem. Ref. Data, Monograph* **9**.
Ciesla F. J. (2008) Radial transport in the solar nebula: Implications for moderately volatile element depletions in chondritic meteorites. *Meteorit. Planet. Sci.* **43**, 639–655.
Cohen B. A. and Hewins R. H. (2004) An experimental study of the formation of metallic iron in chondrules. *Geochim. Cosmochim. Acta* **68**, 1677–1689.
Connolly H. C., Hewins R. H., Ash R. D., Zanda B., Lofgren G. E. and Bourot-Denise M. (1994) Carbon and the formation of reduced chondrules. *Nature* **371**, 136–139.
Cuzzi J. N. and Alexander C. M. O'D. (2006) Chondrule formation in particle-rich nebular regions at least hundreds of kilometres across. *Nature* **441**, 483–485.
Davidson J., Alexander C. M. O'D., Stroud R. M., Busemann H. and Nittler L. R. (2019) Mineralogy and petrology of Dominion Range 08006: A very primitive CO3 carbonaceous chondrite. *Geochim. Cosmochim. Acta* **265**, 259–278.
Davis, A. M., Alexander, C. M. O'. D., Nagahara, H. and Richter, F. M. (2005) Evaporation and condensation during CAI and chondrule formation, Chondrites and the protoplanetary disk, p. 432.
Deloule E. and Robert F. (1995) Interstellar water in meteorites?. *Geochim. Cosmochim. Acta* **59** 4695–4706.
Deloule E., Robert F. and Doukhan J. C. (1998) Interstellar hydroxyl in meteoritic chondrules: implications for the origin of water in the inner solar system. *Geochim. Cosmochim. Acta* **62**, 3367–3378.
Demouchy S. and Mackwell S. (2006) Mechanisms of hydrogen incorporation and diffusion in iron-bearing olivine. *Phys. Chem. Miner.* **33**, 347–355.
Desch S. J. and Connolly H. C. J. (2002) A model of the thermal processing of particles in solar nebula shocks: Application to the cooling rates of chondrules. *Meteorit. Planet. Sci.* **37**, 183–207.
Dixon J. E., Stolper E. M. and Holloway J. R. (1995) An experimental study of water and carbon dioxide solubilities in mid-ocean ridge basaltic liquids. Part I: calibration and solubility models. *J. Petrol.* **36**, 1607–1631.
Doremus R. H. (1994) *Glass science*, 2nd ed. John Wiley & Sons, New York.
Ebel D. S. and Grossman L. (2000) Condensation in dust-enriched systems. *Geochim. Cosmochim. Acta* **64**, 339–366.
Ebel D. S., Libourel G. and Alexander C. M. O'D. (2018) Vapor-melt exchange: constraints on chondrite formation conditions and processes. In *Chondrules Records of Protoplanetary Disk Processes* (eds. S. S. Russel, H. C. Connolly and A. N. Krot). Cambridge University Press, Cambridge, pp. 151–174.
Fedkin A. V. and Grossman L. (2013) Vapor saturation of sodium: Key to unlocking the origin of chondrules. *Geochim. Cosmochim. Acta* **112**, 226–250.
Fortin M.-A., Riddle J., Desjardins-Langlais Y. and Baker D. R. (2015) The effect of water on the sulfur concentration at sulfide saturation (SCSS) in natural melts. *Geochim. Cosmochim. Acta* **160**, 100–116.
Fujiya W., Hoppe P., Ushikubo T., Fukuda K., Lindgren P., Lee M. R., Koike M., Shirai K. and Sano Y. (2019) Migration of D-type asteroids from the outer Solar System inferred from carbonate in meteorites. *Nature Astronomy* **3**, 910–915.

Gaetani G. A., O'Leary J. A., Shimizu N., Bucholz C. E. and Newville M. (2012) Rapid reequilibration of H2O and oxygen fugacity in olivine-hosted melt inclusions. *Geology* **40**, 915–918.

Grossman J. N., Alexander C. M. O'D., Wang J. and Brearley A. J. (2000) Bleached chondrules: Evidence for widespread aqueous processes on the parent asteroids of ordinary chondrites. *Meteorit. Planet. Sci.* **35**, 467–486.

Grossman J. N., Alexander C. M. O'D., Wang J. and Brearley A. J. (2002) Zoned chondrules in Semarkona: Evidence for high-and low-temperature processing. *Meteorit. Planet. Sci.* **37**, 49–73.

Grossman J. N. and Brearley A. J. (2005) The onset of metamorphism in ordinary and carbonaceous chondrites. *Meteorit. Planet. Sci.* **40**, 87–122.

Grossman J. N. and Wasson J. T. (1983) The compositions of chondrules in unequilibrated chondrites an evaluation of models for the formation of chondrules and their precursor materials. *Chondrules Origins*, 88–121.

Grossman J. N. and Wasson J. T. (1985) The origin and history of the metal and sulfide components of chondrules. *Geochim. Cosmochim. Acta* **49**, 925–939.

Halliday A. N. (2013) The origins of volatiles in the terrestrial planets. *Geochim. Cosmochim. Acta* **105**, 146–171.

Hanon P., Robert F. and Chaussidon M. (1998) High carbon concentrations in meteoritic chondrules: A record of metal-silicate differentiation. *Geochim. Cosmochim. Acta* **62**, 903–913.

Hauri E. H., Gaetani G. A. and Green T. H. (2006) Partitioning of water during melting of the Earth's upper mantle at $H_2O$-undersaturated conditions. *Earth Planet. Sci. Lett.* **248**, 715–734.

Hauri E. H., Maclennan J., McKenzie D., Gronvold K., Oskarsson N. and Shimizu N. (2018) $CO_2$ content beneath northern Iceland and the variability of mantle carbon. *Geology* **46**, 55–58.

Hauri E. H., Wang J. H., Dixon J. E., King P. L., Mandeville C. and Newman S. (2002) SIMS analysis of volatiles in silicate glasses: 1. Calibration, matrix effects and comparisons with FTIR. *Chem. Geol.* **183**, 99–114.

Hewins R. H. and Connolly H. C. (1996) Peak Temperatures of Flash-melted Chondrules. In *Chondrules and the Protoplanetary Disk* (eds. R. H. Hewins and E. R. D. Scott). Cambridge Univ. Press, New York, New York, USA, pp. 197–204.

Hewins, R. H., Connolly, H. C., Lofgren Jr, G. E. and Libourel, G. (2005) Experimental constraints on chondrule formation In A. N. Krot, E. R. D. Scott, B. Reipurth (Eds.), Chondrites and the protoplanetary disk, Astronomical Society of the Pacific Conference Series, pp. 286-316.

Hewins R. H., Yu Y., Zanda B. and Bourot-Denise M. (1997) Do nebular fractionations, evaporative losses, or both, influence chondrule compositions? *Antarctic Meteorite Res.* **10**, 275.

Hewins R. H., Zanda B. and Bendersky C. (2012) Evaporation and recondensation of sodium in Semarkona Type II chondrules. *Geochim. Cosmochim. Acta* **78**, 1–17.

Hirschmann M. M., Withers A. C., Ardia P. and Foley N. T. (2012) Solubility of molecular hydrogen in silicate melts and consequences for volatile evolution of terrestrial planets. *Earth Planet. Sci. Lett.* **345**, 38–48.

Horner J., Mousis O. and Hersant F. (2007) Constraints on the formation regions of comets from their D: H ratios. *Earth, Moon, and Planets* **100**, 43–56.

Hudak M. R. and Bindeman I. N. (2020) Solubility, diffusivity, and O isotope systematics of H2O in rhyolitic glass in hydrothermal temperature experiments. *Geochim. Cosmochim. Acta* **283**, 222–242.

Hutchison R., Alexander C. M. O'D. and Barber D. J. (1987) The Semarkona meteorite: First recorded occurrence of smectite in an ordinary chondrite, and its implications. *Geochim. Cosmochim. Acta* **51**, 1875–1882.

Jones R. H. (1990) Petrology and mineralogy of type II, FeO-rich chondrules in Semarkona (LL3. 0): Origin by closed-system fractional crystallization, with evidence for supercooling. *Geochim. Cosmochim. Acta* **54**, 1785–1802.

Jones R. H. (1994) Petrology of FeO-poor, porphyritic pyroxene chondrules in the Semarkona chondrite. *Geochim. Cosmochim. Acta* **58**, 5325–5340.

Jones R. H. (1996) FeO-rich, porphyritic pyroxene chondrules in unequilibrated ordinary chondrites. *Geochim. Cosmochim. Acta* **60**, 3115–3138.

Jones R. H. and Scott E. R. D. (1989) Petrology and thermal history of type IA chondrules in the Semarkona (LL3. 0) chondrite. *Proc. 19th Lunar Planet. Sci. Conf.*, 523–536.

Joung M. K. R., Mac Low M.-M. and Ebel D. S. (2004) Chondrule formation and protoplanetary disk heating by current sheets in nonideal magnetohydrodynamic turbulence. *Astrophys. J.* **606**, 532.

Kennedy A. K., Lofgren G. E. and Wasserburg G. J. (1993) An experimental study of trace element partitioning between olivine, orthopyroxene and melt in chondrules: equilibrium values and kinetic effects. *Earth Planet. Sci. Lett.* **115**, 177–195.

Kimura M., Grossman J. N. and Weisberg M. (2008) Fe-Ni metal in primitive chondrites: Indicators of classification and metamorphic conditions for ordinary and CO chondrites. *Meteorit. Planet. Sci.* **43**, 1161–1177.

Kita N. T., Nagahara H., Tachibana S., Tomomura S., Spicuzza M. J., Fournelle J. H. and Valley J. W. (2010) High precision SIMS oxygen three isotope study of chondrules in LL3 chondrites: Role of ambient gas during chondrule formation. *Geochim. Cosmochim. Acta* **74**, 6610–6635.

Kita N. T. and Ushikubo T. (2012) Evolution of protoplanetary disk inferred from 26Al chronology of individual chondrules. *Meteorit. Planet. Sci.* **47**, 1108–1119.

Koga K., Hauri E. H., Hirschmann M. M. and Bell D. (2003) Hydrogen concentration analyses using SIMS and FTIR: comparison and calibration for nominally anhydrous minerals. *Geochem. Geophys. Geosys.* **4**.

Kohlstedt D. L. and Mackwell S. J. (1998) Diffusion of hydrogen and intrinsic point defects in olivine. *Zeitschrift für physikalische Chemie* **207**, 147–162.

Kong P. and Palme H. (1999) Compositional and genetic relationship between chondrules, chondrule rims, metal, and matrix in the Renazzo chondrite. *Geochim. Cosmochim. Acta* **63**, 3673–3682.

Krot A. N., Libourel G., Goodrich C. A. and Petaev M. I. (2004) Silica-rich igneous rims around magnesian chondrules in CR carbonaceous chondrites: Evidence for condensation origin from fractionated nebular gas. *Meteorit. Planet. Sci.* **39**, 1931–1955.

Krot A. N., Zolensky M. E., Wasson J. T., Scott E. R., Keil K. and Ohsumi K. (1997) Carbide-magnetite assemblages in type-3 ordinary chondrites. *Geochim. Cosmochim. Acta* **61**, 219–237.

Kruijer T. S., Burkhardt C., Budde G. and Kleine T. (2017) Age of Jupiter inferred from the distinct genetics and formation times of meteorites. *Proc. Nat. Acad. Sci.* **114**, 6712–6716.

Lauretta D. S., Lodders K. and Fegley B. (1997) Experimental simulations of sulfide formation in the solar nebula. *Science* **277**, 358–360.

Liu Y., Samaha N.-T. and Baker D. R. (2007) Sulfur concentration at sulfide saturation (SCSS) in magmatic silicate melts. *Geochim. Cosmochim. Acta* **71**, 1783–1799.

Long G. L. and Winefordner J. D. (1983) Limit of detection. A closer look at the IUPAC definition. *Analy. Chem.* **55**, 712A–724A.

MacPherson G. J. (2014) Calcium-Aluminum-Rich Inclusions in Chondritic Meteorites. In *Treatise on Geochemistry* (ed. A. M. Davis). Elsevier, Oxford, pp. 139–179.

Marrocchi Y. and Libourel G. (2013) Sulfur and sulfides in chondrules. *Geochim. Cosmochim. Acta* **119**, 117–136.

Marty B. (2012) The origins and concentrations of water, carbon, nitrogen and noble gases on Earth. *Earth Planet. Sci. Lett.* **313**, 56–66.

Matsunami S., Ninagawa K., Nishimura S., Kubono N., Yamamoto I., Kohata M., Wada T., Yamashita Y., Lu J. and Sears D. W. G. (1993) Thermoluminescence and compositional zoning in the mesostasis of a Semarkona group A1 chondrule and new insights into the chondrule-forming process. *Geochim. Cosmochim. Acta* **57**, 2101–2110.

Mavrogenes J. A. and O'Neill H. S. C. (1999) The relative effects of pressure, temperature and oxygen fugacity on the solubility of sulfide in mafic magmas. *Geochim. Cosmochim. Acta* **63**, 1173–1180.

Mosenfelder J. L., Deligne N. I., Asimow P. D. and Rossman G. R. (2006) Hydrogen incorporation in olivine from 2–12 GPa. *Am. Mineral.* **91**, 285–294.

Mungall J. E. and Martin R. F. (1994) Severe leaching of trachytic glass without devitrification, Terceira, Azores. *Geochim. Cosmochim. Acta* **58**, 75–83.

Nagahara H., Kita N. T., Ozawa K. and Morishita Y. (2008) Condensation of major elements during chondrule formation and its implication to the origin of chondrules. *Geochim. Cosmochim. Acta* **72**, 1442–1465.

Nettles J. W., Lofgren G. E., Carlson W. D. and McSween, Jr, H. Y. (2006) Extent of chondrule melting: Evaluation of experimental textures, nominal grain size, and convolution index. *Meteorit. Planet. Sci.* **41**, 1059–1071.

Newcombe M. E., Brett A., Beckett J. R., Baker M. B., Newman S., Guan Y., Eiler J. M. and Stolper E. M. (2017) Solubility of water in lunar basalt at low pH2O. *Geochim. Cosmochim. Acta* **200**, 330–352.

Nittler L. R., Alexander C. M. O'D., Davidson J., Riebe M. E., Stroud R. M. and Wang J. (2018) High abundances of presolar grains and 15N-rich organic matter in CO3. 0 chondrite dominion range 08006. *Geochim. Cosmochim. Acta* **226**, 107–131.

Palme, H., Lodders, K. and Jones, A. (2014) Solar system abundances of the elements. Planets, Asteriods, Comets and The Solar System, Volume 2 of Treatise on Geochemistry (Second Edition). Edited by Andrew M. Davis. Elsevier, 2014., p. 15-36 2.

Palme H. and O'Neill H. S. C. (2014) Cosmochemical Estimates of Mantle Composition. In *Treatise on Geochemistry* (ed. R. W. Carlson), 2nd ed. Elsevier, pp. 1–38.

Piani L., Marrocchi Y., Libourel G. and Tissandier L. (2016) Magmatic sulfides in the porphyritic chondrules of EH enstatite chondrites. *Geochim. Cosmochim. Acta* **195**, 84–99.

Piani L., Marrocchi Y., Rigaudier T., Vacher L. G., Thomassin D. and Marty B. (2020) Earth's water may have been inherited from material similar to enstatite chondrite meteorites. *Science* **369**, 1110–1113.

Piani L., Robert F. and Remusat L. (2015) Micron-scale D/H heterogeneity in chondrite matrices: A signature of the pristine solar system water? *Earth Planet Sci. Lett.* **415**, 154–164.

Piani L., Yurimoto H. and Remusat L. (2018) A dual origin for water in carbonaceous asteroids revealed by CM chondrites. *Nature astronomy* **2**, 317.

Robert F. (2001) The origin of water on Earth. *Science* **293**, 1056–1058.

Robert F., Javoy M., Halbout J., Dimon B. and Merlivat L. (1987) Hydrogen isotope abundances in the solar system. Part I: Unequilibrated chondrites. *Geochim. Cosmochim. Acta* **51**, 1787–1805.

Roeder P. L. and Emslie R. F. (1970) Olivine-liquid equilibrium. *Contrib. Mineral. Petrol.* **29**, 275–289.

Rosenthal A., Hauri E. H. and Hirschmann M. M. (2015) Experimental determination of C, F, and H partitioning between mantle minerals and carbonated basalt, $CO_2$/Ba and $CO_2$/Nb systematics of partial melting, and the $CO_2$ contents of basaltic source regions. *Earth Planet. Sci. Lett.* **412**, 77–87.

Rubin A. E. (1992) A shock-metamorphic model for silicate darkening and compositionally variable plagioclase in CK and ordinary chondrites. *Geochim. Cosmochim. Acta* **56**, 1705–1714.

Rubin A. E., Sailer A. L. and Wasson J. T. (1999) Troilite in the chondrules of type-3 ordinary chondrites: Implications for chondrule formation. *Geochim. Cosmochim. Acta* **63**, 2281–2298.

Sarafian A. R., Nielsen S. G., Marschall H. R., Gaetani G. A., Righter K. and Berger E. L. (2019) The water and fluorine content of 4 Vesta. *Geochim. Cosmochim. Acta* **266**, 568–581.

Schaefer L. and Fegley, Jr, B. (2010) Chemistry of atmospheres formed during accretion of the Earth and other terrestrial planets. *Icarus* **208**, 438–448.

Schrader D. L., Nagashima K., Krot A. N., Ogliore R. C., Yin Q.-Z., Amelin Y., Stirling C. H. and Kaltenbach A. (2017) Distribution of 26Al in the CR chondrite chondrule-forming region of the protoplanetary disk. *Geochim. Cosmochim. Acta* **201**, 275–302.

Scott E. R. D., Taylor G. J., Rubin A. E., Okada A. and Keil K. (1981) Graphite–magnetite aggregates in ordinary chondritic meteorites. *Nature* **291**, 544–546.

Sears D. W. G., Morse A. D., Hutchison R., Guimon R. K., Jie L., Alexander C. M. O'D., Benoit P. H., Wright I., Pillinger C. and Xie T. (1995) Metamorphism and aqueous alteration in low petrographic type ordinary chondrites. *Meteoritics* **30**, 169–181.

Shu F. H., Shang H. and Lee T. (1996) Toward an astrophysical theory of chondrites. *Science* **271**, 1545–1552.

Smythe D. J., Wood B. J. and Kiseeva E. S. (2017) The S content of silicate melts at sulfide saturation: new experiments and a model incorporating the effects of sulfide composition. *Am. Mineral.* **102**, 795–803.

Stephant A., Remusat L. and Robert F. (2017) Water in type I chondrules of Paris CM chondrite. *Geochim. Cosmochim. Acta* **199**, 75–90.

Sutton S., Bryant A., Lanzirotti A., Newville M. and Cloutis E. (2017) The bulk valence state of Fe and the origin of water in chondrites. *Geochim. Cosmochim. Acta* **211**, 115–132.

Tachibana S. and Huss G. R. (2005) Sulfur isotope composition of putative primary troilite in chondrules from Bishunpur and Semarkona. *Geochim. Cosmochim. Acta* **69**, 3075–3097.

Tenner T. J., Nakashima D., Ushikubo T., Kita N. T. and Weisberg M. K. (2015) Oxygen isotope ratios of FeO-poor chondrules in CR3 chondrites: Influence of dust enrichment and H2O during chondrule formation. *Geochim. Cosmochim. Acta* **148**, 228–250.

Tenner T. J., Nakashima D., Ushikubo T., Tomioka N., Kimura M., Weisberg M. K. and Kita N. T. (2019) Extended chondrule formation intervals in distinct physicochemical environments: Evidence from Al-Mg isotope systematics of CR chondrite chondrules with unaltered plagioclase. *Geochim. Cosmochim. Acta* **260**, 133–160.

Villeneuve J., Libourel G. and Soulié C. (2015) Relationships between type I and type II chondrules: Implications on chondrule formation processes. *Geochim. Cosmochim. Acta* **160**, 277–305.

Wai C. M. and Wasson J. T. (1977) Nebular condensation of moderately volatile elements and their abundances in ordinary chondrites. *Earth Planet. Sci. Lett.* **36**, 1–13.

Warren P. H. (2011) Stable-isotopic anomalies and the accretionary assemblage of the Earth and Mars: A subordinate role for carbonaceous chondrites. *Earth Planet. Sci. Lett.* **311**, 93–100.

Wasson J. T. and Chou C. L. (1974) Fractionation of moderately volatile elements in ordinary chondrites. *Meteoritics* **9**, 69–84.

Wasson J. T. and Kallemeyn G. W. (1988) Compositions of chondrites. *Phil. Trans. Royal Soc. London. Series A Math. Phys. Sci.* **325**, 535–544.

Wood B. J., Smythe D. J. and Harrison T. (2019) The condensation temperatures of the elements: A reappraisal. *Am. Mineral.* **104**, 844–856.

Yanai K., Itoh S., Greenwood J. P. and Yurimoto H. (2012) H2O contents and hydrogen isotopic composition of apatite crystals from L, LL5-6 ordinary chondrites. *Nat. Inst. Polar. Res.*, E37.

Yang L., Ciesla F. J. and Alexander C. M. O'D. (2013) The D/H ratio of water in the solar nebula during its formation and evolution. *Icarus* **226**, 256–267.

Zanda B., Bourot-Denise M. and Hewins R. H. (1995) Condensate sulfide and its metamorphic transformations in primitive chondrites. *Meteorit. Planet. Sci.* **30**, A605.

Zanda B., Lewin E. and Humayun M. (2018) The chondritic assemblage: complementarity is not a required hypothesis. In *Chondrules: Records of Protoplanetary Disk Processe* (eds. S. S. Russel, H. C. Connolly and A. N. Krot). Cambridge University Press, Cambridge, pp. 122–150.

Zhang C. and Duan Z. (2009) A model for C-O–H fluid in the Earth's mantle. *Geochim. Cosmochim. Acta* **73**, 2089–2102.

Zhang Y. and Behrens H. (2000) $H_2O$ diffusion in rhyolitic melts and glasses. *Chem. Geol.* **169**, 243–262.

Zhang Y. and Ni H. (2010) Diffusion of H, C, and O components in silicate melts. *Rev. Mineral. Geochem.* **72**, 171–225.

*Associate editor:* Anders Meibom